POE-Based Robot Kinematic Calibration Using Axis Configuration Space and the Adjoint Error Model

Cheng Li, Yuanqing Wu, Harald Löwe, and Zexiang Li, *Fellow, IEEE*

***Abstract*—The product of exponential model based robot calibration approach eliminates parameter discontinuity and simplifies coordinate frame setup, but demands extra effort to normalize twist coordinates and differentiate parameter-varying exponential maps. In this paper, we show that such an endeavor can be exempted by respecting the nonlinear geometry of the joint axis configuration space (ACS), the set of all possible axis locations. We analyze the geometry of the ACS models for prismatic and revolute joints, and treat the errors as Adjoint transformations on joint twists. We propose a novel robot kinematic calibration algorithm based on the ACS and Adjoint error model. It is geometrically intuitive, computationally efficient, and can easily handle additional assumptions on joint axes relations. We present a comparative study with simulations and experiments to show that our algorithm outperforms the existing ones in various aspects.**

***Index Terms*—Adjoint transformation error, axis configuration space (ACS), calibration and identification, kinematics.**

I. Introduction

ROBOTIC systems for 3C (computer, communication, and consumer electronics) manufacturing has become a technology hot spot. Industrial robots can hardly achieve the high absolute accuracy required in typical 3C operations due to environmental, parametric, measurement, and computational imperfections [1]. Fortunately, robot kinematic calibration can effectively remove most of the overall end-effector error [2], thereby substantially improving the robot's accuracy.

Robot calibration consists of four stages: modeling, measurement, identification, and compensation [3]. The successful development of a kinematic calibration algorithm depends highly on the modeling stage, which is concerned with the selection of a proper kinematic model and specification of its parameters for error identification and compensation. We will refer to the space of all possible parameter values as the *error model* to distinguish it from the kinematic model.

The Denavit–Hartenberg (DH) parameters [4] are widely used to parameterize the relative location of each link coordinate frame (with $\mathbf{z}$-axis coinciding with the joint axis) with four parameters. The deviation of DH parameters from nominal values accounts for both joint encoder error (zero offset) and axis misalignment. However, the DH model becomes discontinuous when two neighboring joint axes are nearly parallel [5]. Several modified DH models have been proposed to eliminate such parameter discontinuity, including the Hayati model [5], the Veitschegger model [6], and the complete and parametrically continuous model [7].

The product of exponentials (POE) model with twist coordinate parameters, on the other hand, parameterizes the absolute initial location of each joint axis with six parameters, and the initial joint position with a seventh variable [8]. The twist coordinates vary smoothly with arbitrary change of joint axis location, leading to a continuous parameterization. Only one reference frame and one tool frame are involved. Okamura and Park first employed the *standard POE model* in an iterative least square calibration algorithm [9]. It requires iteratively differentiating the parameter-varying exponential maps, which substantially decreases the runtime performance [10]. Joint twist normalization is needed to counter the magnitude and pitch change caused by an additive twist error update. Later, it is shown that the initial joint position is a redundant parameter and should be excluded from the calibration [10]–[12]. Yang *et al.* proposed a *minimal POE model* that eliminates the magnitude and pitch constraints [13]. Chen *et al.* proposed a *local POE model* based on a multiplicative error of local link frame locations, which removes all parameter-varying differentiations [14]. Parameter redundancy arises in its nonuniqueness of local frame locations [10].

Schröer *et al.* used three criteria for evaluating the choice of parameters for a robot kinematic model: completeness, continuity, and minimality [15]. The DH model is a complete parameterization in the sense that any possible robot geometry can be described by at least one set of DH parameters. It is discontinuous for near parallel neighboring axes, and minimal because the number of DH parameters equals the maximal number of identifiable parameters $4r + 2t + 6$ [16]–[18], where r and t are the number of revolute and prismatic joints, respectively. The numbers 4, 2, and 6 correspond to the minimal number of parameters needed to determine the initial location of a revolute joint axis,

Manuscript received April 3, 2015; revised November 17, 2015 and April 20, 2016; accepted May 3, 2016. This paper was recommended for publication by Associate Editor A. Mueller and Editor C. Torras upon evaluation of the reviewers' comments. This work was supported in part by Research Grants Council under Grant 615212, Grant 16205614, and Grant 16205915; in part by Shenzhen Municipal Science and Technology Planning Program for Basic Research JCYJ20120618150931822; and in part by National Natural Science Foundation under Grant 51375413. The work of Y. Wu was supported by the PRIN under Grant 20124SMZ88 of the Italian Ministry of Education, Universities and Research.

C. Li was with the Department of Electronic and Computer Engineering, Hong Kong University of Science and Technology, Clear Water Bay, Hong Kong. He is now with the ABB Corporate Research Center, Shanghai 201319, China (e-mail: lichengemail@gmail.com).

Z. Li is with the Department of Electronic and Computer Engineering, Hong Kong University of Science and Technology, Clear Water Bay, Hong Kong (e-mail: eezxli@ust.hk).

Y. Wu is with the Department of Industrial Engineering, University of Bologna, Bologna 40126, Italy (e-mail: yuanqing.wu@unibo.it).

H. Löwe is with the Institut Computational Mathematics, Technical University of Brauschweig, Braunschweig 38106, Deutschland (e-mail: h.loewe@tubs.de).

Color versions of one or more of the figures in this paper are available online at http://ieeexplore.ieee.org.

Digital Object Identifier 10.1109/TRO.2016.2593042

a prismatic joint axis, and the tool frame initial location with respect to the reference frame, respectively. In fact, this number is uniquely determined by the geometric property of the serial manipulator and should not depend on the choice of parameters. He *et al.* attempted to prove that there are $6r + 3t + 6$ identifiable parameters in the standard POE model [19], but overlooked the magnitude and pitch constraints. In [12] we proved that in fact only $4r + 2t + 6$ parameters are identifiable with end-effector pose measurements. The same conclusion can be drawn from the minimal POE model [13] and the *reformulated local POE model* (RLPOE) proposed in [20].

From a geometric viewpoint, any modeling convention is a parameterization of the underlying axis configuration space (ACS), the set of all possible joint axis configurations. It is claimed that a single minimal and complete parameterization cannot exist due to fundamental topological reasons concerning mappings from Euclidean vector spaces to spheres [15], [21]. However, only the ACS of a prismatic joint can be characterized by a sphere (the unit 2-sphere $\mathbf{S}^2 \subset \mathbb{R}^3$). The ACS of a revolute joint is not a 4-sphere $\mathbf{S}^4 \subset \mathbb{R}^5$, and is in fact never explicitly identified in the literature. As we will show in this paper, the ACS of a revolute joint can be identified with the tangent bundle $\mathbf{T}(\mathbf{S}^2)$ of $\mathbf{S}^2$, a four-dimensional (4-D) nonlinear manifold that cannot be covered by a single coordinate neighborhood. It is exactly this topological property that prevents us from defining a single complete and minimal parameterization, either by elementary transformations [15] or by POE-based methods [9], [13], [20].

By treating the prismatic and revolute ACSs as nonlinear manifolds, we can systematically identify the discontinuity and redundancy of any parameterization for a robot kinematic model. A criterion different from Schröer *et al.*'s [15] is advocated in this paper: it is preferable to choose suitable local coordinates for each particular joint axis configuration instead of fixing only one global parameterization. Based on the ACS model, we reformulate the POE-based calibration algorithm by introducing a multiplicative Adjoint transformation error of the twist coordinates, referred to as the *Adjoint error*. This novel algorithm is geometrically intuitive and has a well-structured error Jacobian matrix, with which the identifiability using either pose or point measurements are rigorously proved with a lower bound on the number of samplings. Constraints resulting from both parameter redundancy of the twist coordinate and additional geometric assumptions on joint axis relations are naturally eliminated. Moreover, various kinematic models and calibration algorithms can be conveniently transformed into this *ACS model with Adjoint error* framework for a consistent comparative study. We will show that our calibration algorithm outperforms the others in terms of efficiency, robustness, and ease of implementation. Part of the results has been presented at IEEE ICRA 2014 [10], [12].

This paper is organized as follows. In Section II, we analyze the geometry of the joint ACS with its associated error model. In Section III, we introduce a multiplicative error model for joint twists and the initial tool frame offset, and derive the corresponding kinematic calibration algorithm. In Section IV, we show how our algorithm can be generalized to include some additional constraints on joint axes. In Section V, we give a comparative study of different error models and calibration methods to illustrate the many advantages of our approach. Simulations and experiments are presented in Section VI to support our claims. We conclude our paper in Section VII.

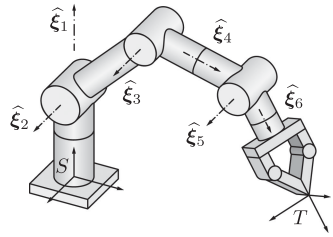

Fig. 1. Notations and convention of robot arm kinematic geometry.

II. Joint Axis Configuration Space and its Associated Adjoint Error Model

A. Robot Forward Kinematic Model Using the POE Formula

We assume the readers are familiar with the special orthogonal group $\mathbf{SO(3)}$ and the special Euclidean group $\mathbf{SE(3)}$ (see [8] and [22] for an elementary introduction). We attach a spatial frame S to the robot base link and a tool frame T to the end-effector. The rigid displacement of T with respect to S can be described by a 4×4 homogeneous matrix $\mathbf{g}_{st} \in \mathbf{SE(3)}$ [8]

$$\mathbf{g}_{st} = \begin{pmatrix} \mathbf{R} & \mathbf{p} \\ \mathbf{0}_{1\times 3} & 1 \end{pmatrix} \in \mathbb{R}^{4\times 4}$$

where the 3×3 matrix $\mathbf{R} \in \mathbf{SO(3)}$ is a proper orthogonal matrix describing coordinate axes of T in S and the 3×1 vector $\mathbf{p} \in \mathbb{R}^{\mathbf{3}}$ is the position vector of the origin of T in S. With a harmless abuse of notation, we also write $\mathbf{g}_{st} = (\mathbf{R}, \mathbf{p})$. Coordinates of a point $\mathbf{q}$ in these two frames are related by

$$\tilde{\mathbf{q}}_s = \mathbf{g}_{st}\tilde{\mathbf{q}}_t$$

where $\tilde{\mathbf{q}} \triangleq (\mathbf{q}^{\mathrm{T}}, 1)^{\mathrm{T}} \in \mathbb{R}^4$ represents the homogeneous coordinates of $\mathbf{q} \in \mathbb{R}^{\mathbf{3}}$.

For an n degrees-of-freedom (DoF) manipulator, we associate to each of its n joints a twist $\widehat{\boldsymbol{\xi}}_i, i = 1, \ldots, n$, of the Lie algebra $\mathbf{se(3)}$ of $\mathbf{SE(3)}$, as shown in Fig. 1, as

$$\widehat{\boldsymbol{\xi}}_i = \begin{pmatrix} \widehat{\mathbf{w}}_i & \mathbf{v}_i \\ \mathbf{0}_{1\times 3} & 0 \end{pmatrix} \in \mathbb{R}^{4\times 4}, \quad \mathbf{w}_i, \mathbf{v}_i \in \mathbb{R}^3$$

where $\widehat{\mathbf{w}}_i \in \mathbf{so(3)}$, the Lie algebra of $\mathbf{SO(3)}$, is a 3×3 skew symmetric matrix satisfying $\widehat{\mathbf{w}}_i\mathbf{x} = \mathbf{w}_i \times \mathbf{x}, \forall \mathbf{x} \in \mathbb{R}^3$ [8]. $\widehat{\boldsymbol{\xi}}_i$ can be identified with the 6×1 vector $\boldsymbol{\xi}_i = (\mathbf{v}_i^{\mathrm{T}}, \mathbf{w}_i^{\mathrm{T}})^{\mathrm{T}} \in \mathbb{R}^6$. For a revolute joint, $\mathbf{w}_i, \|\mathbf{w}_i\| = 1$ gives the unit direction of the joint axis and $\mathbf{v}_i = \mathbf{q}_i \times \mathbf{w}_i$, where $\mathbf{q}_i$ is a point on the joint axis; for a prismatic joint, $\mathbf{w}_i = 0$, and $\mathbf{v}_i, \|\mathbf{v}_i\| = 1$ gives the unit direction of the joint axis.

The *forward kinematics* of a serial robot, which maps joint variables $\boldsymbol{\Theta} = (\theta_1, \cdots, \theta_n)^{\mathrm{T}}$ to the tool frame displacement $\mathbf{g}_{st}$, is given by the POE formula [8]

$$\mathbf{g}_{st} = f(\boldsymbol{\Theta}) = e^{\widehat{\boldsymbol{\xi}}_1\theta_1} \cdots e^{\widehat{\boldsymbol{\xi}}_n\theta_n}\mathbf{g}_{st_0}$$

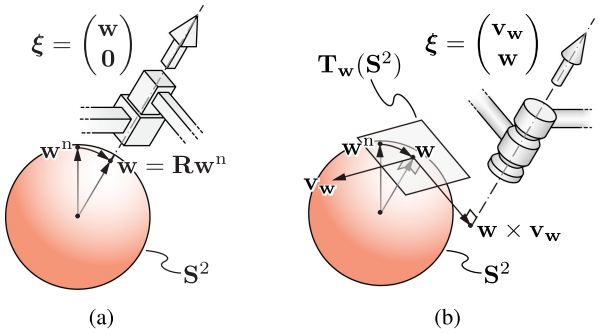

Fig. 2. ACS manifolds of (a) prismatic joint $\mathscr{C}_{\mathcal{P}}$ and (b) revolute joint $\mathscr{C}_{\mathcal{R}}$.

where the matrix exponential $e^{\widehat{\boldsymbol{\xi}}_i \theta_i} \triangleq \exp(\widehat{\boldsymbol{\xi}}_i \theta_i)$ is the motion generated by joint i with joint variable θ_i, and $\mathbf{g}_{st_0}$ denotes the initial tool frame displacement.

B. Geometric ACS Model and its Associated Error Model

1) Prismatic Joints: A particular axis configuration of a prismatic joint $\mathcal{P}$ is unambiguously characterized by a free unit vector $\mathbf{w} \in \mathbb{R}^3, \|\mathbf{w}\| = 1$, as shown in Fig. 2(a). Therefore, the ACS of a prismatic joint, denoted by $\mathscr{C}_{\mathcal{P}}$, is the unit 2-sphere $\mathbf{S}^2$ [15]. The joint twist coordinates corresponding to $\mathbf{w} \in \mathbf{S}^2$ are given by $\boldsymbol{\xi} = (\mathbf{w}^{\mathrm{T}}, \mathbf{0}_{1\times 3})^{\mathrm{T}}$.

In respect to the nonlinear geometry of $\mathbf{S}^2$, a deviation from the nominal configuration $\mathbf{w}^{\mathrm{n}}$ to the actual configuration $\mathbf{w}^{\mathrm{a}}$ should not be expressed in an additive form as implemented in [9] as

$$\mathbf{w}^{\mathrm{a}} = \mathbf{w}^{\mathrm{n}} + \delta\mathbf{w}, \quad \|\mathbf{w}^{\mathrm{a}}\| = 1$$

but instead in the multiplicative form

$$\mathbf{w}^{\mathrm{a}} = \mathbf{R}\mathbf{w}^{\mathrm{n}}, \quad \mathbf{R} \in \mathbf{SO(3)}.$$

Since $\mathbf{R}$ is orthonormal,

$$(\mathbf{w}^{\mathrm{a}})^{\mathrm{T}}\mathbf{w}^{\mathrm{a}} = (\mathbf{w}^{\mathrm{n}})^{\mathrm{T}}\mathbf{R}^{\mathrm{T}}\mathbf{R}\mathbf{w}^{\mathrm{n}} = (\mathbf{w}^{\mathrm{n}})^{\mathrm{T}}\mathbf{w}^{\mathrm{n}} = 1$$

the quadratic constraint $\|\mathbf{w}^{\mathrm{a}}\| = 1$ is automatically satisfied. This multiplicative error model for $\mathscr{C}_{\mathcal{P}}$ is naturally summarized by the *transitive action*[1] of $\mathbf{SO(3)}$ on $\mathbf{S}^2$ as

$$\begin{aligned} \Psi_{\mathcal{P}} : \mathbf{SO(3)} \times \mathbf{S}^2 &\to \mathbf{S}^2 \\ (\mathbf{R}, \mathbf{w}) &\mapsto \mathbf{R}\mathbf{w}. \end{aligned} \tag{1}$$

Transitivity of $\Psi_{\mathcal{P}}$ is equivalent to the fact that any deviation of any nominal axis $\mathbf{w}^{\mathrm{n}} \in \mathbf{S}^2$ can be expressed by (1).

2) Revolute Joints: The axis of a revolute joint $\mathcal{R}$ (or more generally, a helical joint $\mathcal{H}$) is no longer a free vector $\mathbf{w} \in \mathbf{S}^2$, but a directed spatial line with twist coordinates $\boldsymbol{\xi} = (\mathbf{v}_{\mathbf{w}}^{\mathrm{T}}, \mathbf{w}^{\mathrm{T}})^{\mathrm{T}}$ satisfying the following constraints:[2]

$$\begin{cases} \mathbf{w}^{\mathrm{T}}\mathbf{w} &= 1 \quad (2) \\ \mathbf{w}^{\mathrm{T}}\mathbf{v}_{\mathbf{w}} &= 0 \quad (3) \end{cases}$$

which shows that the ACS of a revolute joint, denoted by $\mathscr{C}_{\mathcal{R}}$, is in one-to-one correspondence with the set of all tangent vectors $\mathbf{v}_{\mathbf{w}}$ at all points $\mathbf{w}$ of $\mathbf{S}^2$, or the tangent bundle $\mathbf{T}(\mathbf{S}^2)$ of $\mathbf{S}^2$, as shown in Fig. 2(b) as

$$\mathbf{T}(\mathbf{S}^2) \triangleq \{(\mathbf{w}, \mathbf{v}_{\mathbf{w}}) \in \mathbf{S}^2 \times \mathbb{R}^3 | \mathbf{w}^{\mathrm{T}}\mathbf{v}_{\mathbf{w}} = 0\}. \tag{4}$$

Since the tangent plane $\mathbf{T}_{\mathbf{w}}(\mathbf{S}^2) \triangleq \{\mathbf{v}_{\mathbf{w}} \in \mathbb{R}^3 | \mathbf{w}^{\mathrm{T}}\mathbf{v}_{\mathbf{w}} = 0\}$ at each point $\mathbf{w} \in \mathbf{S}^2$ is isomorphic to $\mathbb{R}^2$, and $\mathbf{S}^2$ is a two-dimensional (2-D) manifold, $\mathbf{T}(\mathbf{S}^2)$ is a 4-D manifold. However, it should be distinguished from the product space $\mathbf{S}^2 \times \mathbb{R}^2$: a separate parameterization of $\mathbf{S}^2$ and $\mathbb{R}^2$ does not lead to a correct parameterization of $\mathbf{T}(\mathbf{S}^2)$ [25, Th. 7.5.13]. Schröer *et al.* [15] suggest using the extended space $\mathscr{C}_{\mathcal{R}} \times \mathbb{R} \simeq \mathbf{S}^2 \times \mathbb{R}^3$; that is, ignoring the constraint in (4), to help describe the revolute ACS, but does not utilize it in deriving the error model.

We develop the error model for revolute joints that respects the geometry of $\mathbf{T}(\mathbf{S}^2)$ as follows. By differentiating $\Psi_{\mathcal{P}}$ in (1), we obtain

$$\begin{aligned} \Psi_{\mathcal{R}} : \mathbf{T}(\mathbf{SO(3)}) \times \mathbf{T}(\mathbf{S}^2) &\to \mathbf{T}(\mathbf{S}^2) \\ ((\mathbf{R}, \mathbf{V}_{\mathbf{R}}), (\mathbf{w}, \mathbf{v}_{\mathbf{w}})) &\mapsto (\mathbf{R}\mathbf{w}, \underbrace{\mathbf{V}_{\mathbf{R}}\mathbf{w} + \mathbf{R}\mathbf{v}_{\mathbf{w}}}_{\text{Leibniz's product rule}}) \end{aligned} \tag{5}$$

where $\mathbf{V}_{\mathbf{R}} \in \mathbf{T}_{\mathbf{R}}(\mathbf{SO(3)})$ is a 3×3 matrix satisfying $\mathbf{V}_{\mathbf{R}}\mathbf{R}^{\mathrm{T}} \in \mathbf{so(3)}$. Recall that the tangent bundle $\mathbf{T}(\mathbf{G})$ of a Lie group $\mathbf{G}$ with Lie algebra $\mathfrak{g}$ is always trivial, meaning it is diffeomorphic to $\mathbf{G} \times \mathfrak{g}$ via left or right trivialization (see [26, Lemma 9.1.6.(b)]). Therefore, $\mathbf{T}(\mathbf{SO(3)})$ is diffeomorphic to $\mathbf{SO(3)} \times \mathbb{R}^3$ via

$$\begin{aligned} \mathbf{T}(\mathbf{SO(3)}) &\to \mathbf{SO(3)} \times \mathbb{R}^3 \\ (\mathbf{R}, \mathbf{V}_{\mathbf{R}}) &\mapsto (\mathbf{R}, \mathbf{p}), \quad \widehat{\mathbf{p}} = \mathbf{V}_{\mathbf{R}}\mathbf{R}^{\mathrm{T}}. \end{aligned} \tag{6}$$

Moreover, it admits a Lie group structure called a tangent Lie group, under which (5) becomes a transitive action of $\mathbf{T}(\mathbf{SO(3)})$ on $\mathbf{T}(\mathbf{S}^2)$ (see Appendix A for details; see also [26, Example 9.2.24]). Therefore, $\Psi_{\mathcal{R}}$ leads to a natural error model for revolute joints.

Note that the collection of all zero tangent vectors $\mathbf{0}_{\mathbf{w}} \in \mathbf{T}_{\mathbf{w}}(\mathbf{S}^2), \forall \mathbf{w} \in \mathbf{S}^2$ is a 2-D submanifold of $\mathbf{T}(\mathbf{S}^2)$, called the *zero section* as

$$\mathbf{0}_{\mathbf{S}^2} \triangleq \{(\mathbf{w}, \mathbf{0}) \in \mathbf{S}^2 \times \mathbb{R}^3\}$$

which is diffeomorphic to $\mathbf{S}^2$. This unifies the ACSs of $\mathcal{P}$ and $\mathcal{R}$ by identifying $\mathscr{C}_{\mathcal{P}}$ with a submanifold of $\mathscr{C}_{\mathcal{R}}$.

[1] An action of a Lie group $\mathbf{G}$ on a differentiable manifold $\mathbf{M}$ is a smooth map $\Psi : \mathbf{G} \times \mathbf{M} \to \mathbf{M}$ satisfying $\Psi(\mathbf{I}, \mathbf{x}) = \mathbf{x}$ and $\Psi(\mathbf{g}_1, \Psi(\mathbf{g}_2, \mathbf{x})) = \Psi(\mathbf{g}_1\mathbf{g}_2, \mathbf{x})$ for any $\mathbf{x} \in \mathbf{M}$, $\mathbf{g}_1, \mathbf{g}_2 \in \mathbf{G}$ and $\mathbf{I}$ the identity element of $\mathbf{G}$. Ψ is said to be transitive if for any $\mathbf{x}, \mathbf{y} \in \mathbf{M}$ there exists $\mathbf{g} \in \mathbf{G}$, such that $\Psi(\mathbf{g}, \mathbf{x}) = \mathbf{y}$ (see [23, Section III-7]).

[2] A spatial line is uniquely parameterized by homogeneous Plücker coordinates $(\mathbf{w}^{\mathrm{T}}, \mathbf{v}_{\mathbf{w}}^{\mathrm{T}})^{\mathrm{T}} \in \mathbb{R}\mathbf{P}^5$ (five-dimensional real projective space) satisfying homogeneous constraint (3) [24]. In our case, however, $(\mathbf{v}_{\mathbf{w}}^{\mathrm{T}}, \mathbf{w}^{\mathrm{T}})^{\mathrm{T}}$ and $(-\mathbf{v}_{\mathbf{w}}^{\mathrm{T}}, -\mathbf{w}^{\mathrm{T}})^{\mathrm{T}}$ represent two different configurations of the joint axis.

C. $\Psi_{\mathcal{R}}$ and $\Psi_{\mathcal{P}}$ as Adjoint Transformation Error

The transitive action $\Psi_{\mathcal{R}}$ (5) becomes a linear action on $\mathbf{se(3)}$ under twist coordinates

$$\Psi_{\mathcal{R}}\left((\mathbf{R},\mathbf{V_R}),\begin{pmatrix}\mathbf{v_w}\\ \mathbf{w}\end{pmatrix}\right)=\begin{pmatrix}\mathbf{V_R w}+\mathbf{R v_w}\\ \mathbf{R w}\end{pmatrix}=\begin{pmatrix}\mathbf{R} & \widehat{\mathbf{p}}\mathbf{R}\\ \mathbf{0}_{3\times3} & \mathbf{R}\end{pmatrix}\begin{pmatrix}\mathbf{v_w}\\ \mathbf{w}\end{pmatrix} \quad (7)$$

where $\widehat{\mathbf{p}}=\mathbf{V_R}\mathbf{R}^{\mathrm{T}}$ as in (6). One immediately identifies (7) as an *Adjoint transformation* [8], denoted by $\mathbf{Ad_g}$, of the twist $\boldsymbol{\xi}$ with $\mathbf{g}=(\mathbf{R},\mathbf{p})$ as

$$\mathbf{Ad}:\mathbf{SE(3)}\times\mathbf{se(3)}\to\mathbf{se(3)}$$
$$(\mathbf{g},\boldsymbol{\xi})\mapsto\mathbf{Ad_g}\boldsymbol{\xi}=\begin{pmatrix}\mathbf{R} & \widehat{\mathbf{p}}\mathbf{R}\\ \mathbf{0}_{3\times3} & \mathbf{R}\end{pmatrix}\boldsymbol{\xi}. \quad (8)$$

This is not a mere coincidence: it is shown by (6) and Appendix A that $\mathbf{T(SO(3))}$ is isomorphic as a Lie group to $\mathbf{SE(3)}$; and $\Psi_{\mathcal{R}}$ is equivalent to the Adjoint action of $\mathbf{SE(3)}$ on $\mathbf{se(3)}$ restricted to $\mathscr{C}_{\mathcal{R}}$. Physically speaking, we can always consider deviations of joint axes as rigid displacements of the twist coordinates, which are naturally represented by Adjoint transformations [27].

Similarly, $\Psi_{\mathcal{P}}$ is equivalent to the Adjoint action restricted to $\mathscr{C}_{\mathcal{P}}\simeq\mathbf{0}_{\mathbf{S}^2}\subset\mathbf{se(3)}$ as

$$\Psi_{\mathcal{P}}\left((\mathbf{R},\mathbf{V_R}),\begin{pmatrix}\mathbf{w}\\ \mathbf{0}\end{pmatrix}\right)=\begin{pmatrix}\mathbf{R w}\\ \mathbf{0}\end{pmatrix}=\begin{pmatrix}\mathbf{R} & \widehat{\mathbf{p}}\mathbf{R}\\ \mathbf{0}_{3\times3} & \mathbf{R}\end{pmatrix}\begin{pmatrix}\mathbf{w}\\ \mathbf{0}\end{pmatrix}.$$

We emphasize that the Adjoint transformation error (or simply *Adjoint error*) alone does not provide an adequate model. The Adjoint action (8) is not transitive on $\mathbf{se(3)}$; it is necessarily transitive on the ACSs $\mathscr{C}_{\mathcal{R}}$ and $\mathscr{C}_{\mathcal{P}}$, which are simply two orbits of the Adjoint action. Consequently, it does not help to identify and resolve redundancy in the Adjoint transformation, which involves six rather than four (or two) parameters that parameterize the 4-D (2-D) ACS $\mathscr{C}_{\mathcal{R}}$ ($\mathscr{C}_{\mathcal{P}}$).

On the other hand, with the explicit definition of the ACSs $\mathscr{C}_{\mathcal{R}}$ and $\mathscr{C}_{\mathcal{P}}$, the Adjoint action corresponds naturally to the action $\Psi_{\mathcal{R}}$ and $\Psi_{\mathcal{P}}$, respectively, without invoking the quadratic constraints (2) and (3).

D. Minimal Parameterization of $\mathscr{C}_{\mathcal{R}}$ and $\mathscr{C}_{\mathcal{P}}$ by Quotient Space

By the transitivity of $\Psi_{\mathcal{P}}$ and $\Psi_{\mathcal{R}}$ in (1) and (5), the Adjoint action $\mathbf{Ad}$ is also transitive when restricted to $\mathscr{C}_{\mathcal{R}}=\mathbf{T}(\mathbf{S}^2)$ (or $\mathscr{C}_{\mathcal{P}}\simeq\mathbf{0}_{\mathbf{S}^2}$). Therefore, any deviation of the joint axis is equivalent to an Adjoint transformation $\mathbf{Ad_g}$ for some $\mathbf{g}\in\mathbf{SE(3)}$. However, the set of all possible deviations in $\mathscr{C}_{\mathcal{R}}$ (or $\mathscr{C}_{\mathcal{P}}$) is not in one-to-one correspondence with $\mathbf{SE(3)}$: any $\boldsymbol{\xi}\in\mathbf{T}(\mathbf{S}^2)$ as a directed line admits an axial symmetry so that it remains fixed under translation along and rotation about itself. The set of all $\mathbf{g}\in\mathbf{SE(3)}$ that fixes $\boldsymbol{\xi}\in\mathbf{T}(\mathbf{S}^2)$ under Adjoint action forms a 2-D cylindrical subgroup [28] as

$$\mathbf{C}(\boldsymbol{\xi})\triangleq\left\{e^{\hat{\boldsymbol{\xi}}\theta_1+\hat{\mathbf{V}}_{\boldsymbol{\xi}}\theta_2}\,\middle|\,\theta_1,\ \theta_2\in\mathbb{R}\right\},\boldsymbol{\xi}=\begin{pmatrix}\mathbf{v_w}\\ \mathbf{w}\end{pmatrix},\mathbf{V}_{\boldsymbol{\xi}}\triangleq\begin{pmatrix}\mathbf{w}\\ \mathbf{0}\end{pmatrix}. \quad (9)$$

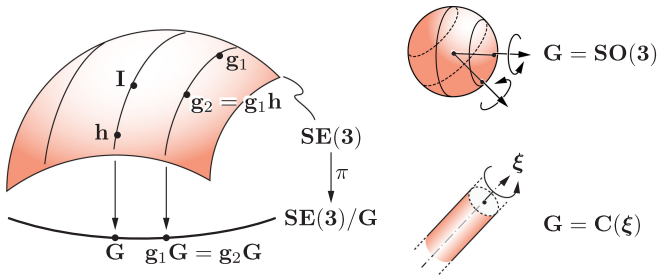

Fig. 3. Illustration of a quotient manifold $\mathbf{SE(3)/G}$ with $\mathbf{G}$ a Lie subgroup of $\mathbf{SE(3)}$. Example one (right top): $\mathbf{S}^2$ with $\mathbf{G}=\mathbf{SO(3)}$; example two (right bottom): an infinitely long cylinder with $\mathbf{G}=\mathbf{C}(\boldsymbol{\xi})$.

$\mathbf{C}(\boldsymbol{\xi})$ is the *isotropy subgroup* of $\boldsymbol{\xi}\in\mathbf{T}(\mathbf{S}^2)$, meaning that

$$\mathbf{Ad}_{\mathbf{g}_1}\boldsymbol{\xi}=\mathbf{Ad}_{\mathbf{g}_2}\boldsymbol{\xi}\quad\text{iff}\quad\mathbf{g}_2=\mathbf{g}_1\mathbf{h},\mathbf{h}\in\mathbf{C}(\boldsymbol{\xi}).$$

In other words, any two rigid displacements $\mathbf{g}_1,\mathbf{g}_2\in\mathbf{SE(3)}$ define the same deviation of $\boldsymbol{\xi}$ if and only if $\mathbf{g}_2=\mathbf{g}_1\mathbf{h}$ for some $\mathbf{h}\in\mathbf{C}(\boldsymbol{\xi})$. Therefore, $\mathscr{C}_{\mathcal{R}}$ is in one-to-one correspondence with the *quotient space* $\mathbf{SE(3)/C}(\boldsymbol{\xi})$ comprising all equivalence classes $\mathbf{gC}(\boldsymbol{\xi})\triangleq\{\mathbf{gh}|\mathbf{h}\in\mathbf{C}(\boldsymbol{\xi})\}$ defined by the equivalence relation

$$\mathbf{g}_1\sim\mathbf{g}_2\quad\text{iff}\quad\mathbf{g}_2\in\mathbf{g}_1\mathbf{C}(\boldsymbol{\xi}).$$

By treating each equivalence class as a single element, $\mathbf{SE(3)/C}(\boldsymbol{\xi})$ becomes a differentiable manifold of dimension $\dim\mathbf{SE(3)}-\dim\mathbf{C}(\boldsymbol{\xi})=6-2=4$ [23, Th. IV.9.2].

Intuitively speaking, a quotient manifold $\mathbf{SE(3)/G}$ with $\mathbf{G}$ a Lie subgroup of $\mathbf{SE(3)}$ offers a rigorous way of removing ineffective displacements (i.e., causing no change in configuration) prescribed by $\mathbf{G}$, such as for the localization of symmetric workpieces [29] and modeling spindle configurations of a five-axis machine [30]: two displacements $\mathbf{g}_1,\mathbf{g}_2\in\mathbf{SE(3)}$ with $\mathbf{g}_2\sim\mathbf{g}_1$ define the same configuration since $\mathbf{G}$ leaves the configuration invariant. Formally, this is characterized by $\mathbf{g}_1$ and $\mathbf{g}_2$ being mapped to the same equivalence class $\mathbf{g}_1\mathbf{G}$ using the following natural projection π (see Fig. 3):

$$\pi:\mathbf{SE(3)}\to\mathbf{SE(3)/G},\quad\mathbf{g}\mapsto\mathbf{gG},\ \mathbf{g}\in\mathbf{SE(3)}$$

if and only if $\mathbf{g}_1\sim\mathbf{g}_2$.

According to [23, Th. IV.9.3], $\mathbf{SE(3)/C}(\boldsymbol{\xi})$ is diffeomorphic to the ACS $\mathscr{C}_{\mathcal{R}}=\mathbf{T}(\mathbf{S}^2)$ via

$$F_{\boldsymbol{\xi}}:\mathbf{SE(3)/C}(\boldsymbol{\xi})\to\mathbf{T}(\mathbf{S}^2)$$
$$\mathbf{gC}(\boldsymbol{\xi})\mapsto\mathbf{Ad_g}\boldsymbol{\xi} \quad (10)$$

for any particular $\boldsymbol{\xi}\in\mathbf{T}(\mathbf{S}^2)$. If G is a local parameterization of the quotient space $\mathbf{SE(3)/C}(\boldsymbol{\xi})$ on a neighborhood of $\mathbf{C}(\boldsymbol{\xi})\in\mathbf{SE(3)/C}(\boldsymbol{\xi})$, then the composition map $F_{\boldsymbol{\xi}}\circ G$ immediately gives a local minimal parameterization of $\mathbf{T}(\mathbf{S}^2)$ on a neighborhood of $\boldsymbol{\xi}\in\mathbf{T}(\mathbf{S}^2)$ as

$$\mathbb{R}^4\xrightarrow{G}\mathbf{SE(3)/C}(\boldsymbol{\xi})\xrightarrow{F_{\boldsymbol{\xi}}}\mathbf{T}(\mathbf{S}^2). \quad (11)$$

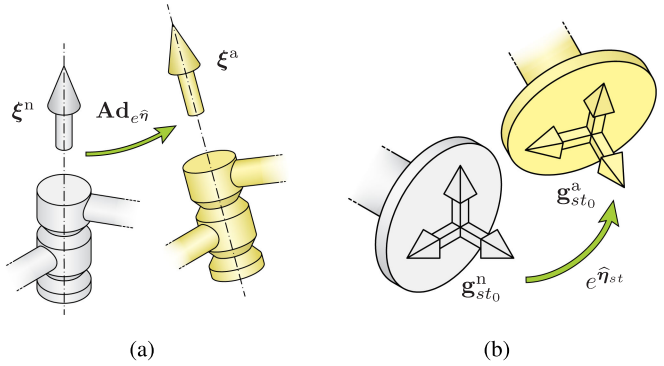

Fig. 4. Error model for (a) joint twists and (b) tool frame offset.

Similarly, the isotropy subgroup of $\boldsymbol{\xi} \in \mathscr{C}_{\mathcal{P}} \simeq \mathbf{0}_{\mathbf{S}^2}$ is the 4-D Schönflies subgroup [28] defined by

$$\begin{aligned}\mathbf{X}(\boldsymbol{\xi}) &\triangleq \left\{ e^{\sum_{i=1}^{3} \widehat{\mathbf{e}}_i \theta_i + \widehat{\mathbf{W}}_{\boldsymbol{\xi}} \theta_4} \,|\, \theta_i \in \mathbb{R}, i = 1, \ldots, 4 \right\} \\ \mathbf{e}_1 &\triangleq \begin{pmatrix} 1 & 0 & 0 & 0 & 0 & 0 \end{pmatrix}^{\mathrm{T}},\ \mathbf{e}_2 \triangleq \begin{pmatrix} 0 & 1 & 0 & 0 & 0 & 0 \end{pmatrix}^{\mathrm{T}} \\ \mathbf{e}_3 &\triangleq \begin{pmatrix} 0 & 0 & 1 & 0 & 0 & 0 \end{pmatrix}^{\mathrm{T}},\ \boldsymbol{\xi} = \begin{pmatrix} \mathbf{w} \\ \mathbf{0} \end{pmatrix}, \mathbf{W}_{\boldsymbol{\xi}} \triangleq \begin{pmatrix} \mathbf{0} \\ \mathbf{w} \end{pmatrix} \end{aligned} \quad (12)$$

and therefore $\mathscr{C}_{\mathcal{P}} \simeq \mathbf{0}_{\mathbf{S}^2}$ is diffeomorphic to the 2-D quotient space $\mathbf{SE}(\mathbf{3})/\mathbf{X}(\boldsymbol{\xi})$ via

$$\begin{aligned} F^0_{\boldsymbol{\xi}} : \mathbf{SE}(\mathbf{3})/\mathbf{X}(\boldsymbol{\xi}) &\to \mathbf{0}_{\mathbf{S}^2} \\ \mathbf{g}\mathbf{X}(\boldsymbol{\xi}) &\mapsto \mathbf{Ad}_{\mathbf{g}}\boldsymbol{\xi}, \quad \boldsymbol{\xi} \in \mathbf{0}_{\mathbf{S}^2}\ . \end{aligned}$$

A similar minimal parameterization for $\mathscr{C}_{\mathcal{P}}$ as in (11) can be defined by

$$\mathbb{R}^2 \xrightarrow{G^0} \mathbf{SE}(\mathbf{3})/\mathbf{X}(\boldsymbol{\xi}) \xrightarrow{F^0_{\boldsymbol{\xi}}} \mathbf{0}_{\mathbf{S}^2}\ . \quad (13)$$

In the next section, we will give specific minimal parameterization of $\mathscr{C}_{\mathcal{R}}$ and $\mathscr{C}_{\mathcal{P}}$ based on (11) and (13), respectively.

III. Calibration Using Adjoint Error Model

A. Adjoint Error Model for Joint Twists

The Adjoint error of a nominal joint twist, as in Fig. 4(a), is given by

$$\boldsymbol{\xi}^{\mathrm{a}} = \mathbf{Ad}_{\mathbf{g}}\boldsymbol{\xi}^{\mathrm{n}} = \mathbf{Ad}_{e^{\widehat{\boldsymbol{\eta}}}}\boldsymbol{\xi}^{\mathrm{n}} \quad (14)$$

for some $\boldsymbol{\eta} = (\mathbf{v}_{\boldsymbol{\eta}}^{\mathrm{T}}, \mathbf{w}_{\boldsymbol{\eta}}^{\mathrm{T}})^{\mathrm{T}} \in \mathbf{se}(\mathbf{3})$, since the exponential map is surjective by Chasles' theorem [8].

A minimal parameterization (11) of the ACS model $\mathscr{C}_{\mathcal{R}}$ may be given by

$$\mathbb{R}^4 \xrightarrow{\iota} \mathbf{se}(\mathbf{3}) \xrightarrow{\exp} \mathbf{SE}(\mathbf{3}) \xrightarrow{\pi} \mathbf{SE}(\mathbf{3})/\mathbf{C}(\boldsymbol{\xi}^{\mathrm{n}}) \xrightarrow{F_{\boldsymbol{\xi}^{\mathrm{n}}}} \mathbf{T}(\mathbf{S}^2) \quad (15)$$

where $G = \pi \circ \exp \circ \iota$ and ι is an injection of $\mathbb{R}^4$ into $\mathbf{se}(\mathbf{3})$. By the inverse function theorem [23], $F_{\boldsymbol{\xi}^{\mathrm{n}}} \circ G$ in (15) defines a local minimal parameterization (local diffeomorphism) of $\mathscr{C}_{\mathcal{R}}$ on a neighborhood of $\boldsymbol{\xi}^{\mathrm{n}}$ as

$$\boldsymbol{\Sigma}_4 \to \mathbf{T}(\mathbf{S}^2), \quad \boldsymbol{\eta} \mapsto \mathbf{Ad}_{e^{\widehat{\boldsymbol{\eta}}}}\boldsymbol{\xi}^{\mathrm{n}}, \quad \boldsymbol{\xi}^{\mathrm{n}} \in \mathbf{T}(\mathbf{S}^2) \quad (16)$$

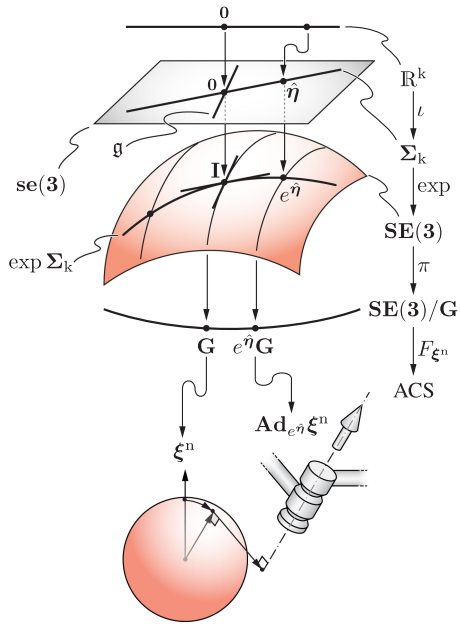

Fig. 5. Minimal parametrization of ACSs. For $\mathrm{ACS} = \mathscr{C}_{\mathcal{R}}$, $\mathbf{G} = \mathbf{C}(\boldsymbol{\xi}^{\mathrm{n}})$, $\mathfrak{g} = \mathfrak{c}(\boldsymbol{\xi}^{\mathrm{n}})$ and $k = 4$; for $\mathrm{ACS} = \mathscr{C}_{\mathcal{P}}$, $\mathbf{G} = \mathbf{X}(\boldsymbol{\xi}^{\mathrm{n}})$, $\mathfrak{g} = \mathfrak{x}(\boldsymbol{\xi}^{\mathrm{n}})$ and $k = 2$.

if and only if the image space $\boldsymbol{\Sigma}_4 \triangleq \mathrm{Im}(\iota)$ of ι is a 4-D vector subspace of $\mathbf{se}(\mathbf{3})$ satisfying

$$\boldsymbol{\Sigma}_4 \oplus \mathfrak{c}(\boldsymbol{\xi}^{\mathrm{n}}) = \mathbf{se}(\mathbf{3}) \quad (17)$$

where $\mathfrak{c}(\boldsymbol{\xi}^{\mathrm{n}})$ is the Lie algebra of $\mathbf{C}(\boldsymbol{\xi}^{\mathrm{n}})$ defined in (9) as

$$\mathfrak{c}(\boldsymbol{\xi}^{\mathrm{n}}) \triangleq \{\boldsymbol{\xi}^{\mathrm{n}}, \mathbf{V}_{\boldsymbol{\xi}^{\mathrm{n}}}\}_{\mathrm{sp}}, \quad \boldsymbol{\xi}^{\mathrm{n}} = \begin{pmatrix} \mathbf{v}^{\mathrm{n}} \\ \mathbf{w}^{\mathrm{n}} \end{pmatrix}, \mathbf{V}_{\boldsymbol{\xi}^{\mathrm{n}}} \triangleq \begin{pmatrix} \mathbf{w}^{\mathrm{n}} \\ \mathbf{0} \end{pmatrix}$$

and $\{\boldsymbol{\xi}^{\mathrm{n}}, \mathbf{V}_{\boldsymbol{\xi}^{\mathrm{n}}}\}_{\mathrm{sp}}$ denotes the space spanned by $\boldsymbol{\xi}^{\mathrm{n}}$ and $\mathbf{V}_{\boldsymbol{\xi}^{\mathrm{n}}}$. In other words, when updating the nominal axis $\boldsymbol{\xi}^{\mathrm{n}}$ with Adjoint error $\mathtt{Ad}_{e^{\widehat{\boldsymbol{\eta}}}}$, $\boldsymbol{\eta}$ should not be a vector in $\mathfrak{c}(\boldsymbol{\xi}^{\mathrm{n}})$ (see Fig. 5). Similarly, a local minimal parameterization (13) of $\mathscr{C}_{\mathcal{P}}$ may be given by

$$\boldsymbol{\Sigma}_2 \to \mathbf{0}_{\mathbf{S}^2}, \quad \boldsymbol{\eta} \mapsto \mathbf{Ad}_{e^{\widehat{\boldsymbol{\eta}}}}\boldsymbol{\xi}^{\mathrm{n}}, \quad \boldsymbol{\xi}^{\mathrm{n}} \in \mathbf{0}_{\mathbf{S}^2}$$

with

$$\boldsymbol{\Sigma}_2 \oplus \mathfrak{x}(\boldsymbol{\xi}^{\mathrm{n}}) = \mathbf{se}(\mathbf{3}) \quad (18)$$

where $\mathfrak{x}(\boldsymbol{\xi}^{\mathrm{n}})$ is the Lie algebra of $\mathbf{X}(\boldsymbol{\xi}^{\mathrm{n}})$ as in (12) as

$$\mathfrak{x}(\boldsymbol{\xi}^{\mathrm{n}}) \triangleq \{\mathbf{e}_1, \mathbf{e}_2, \mathbf{e}_3, \mathbf{W}_{\boldsymbol{\xi}^{\mathrm{n}}}\}_{\mathrm{sp}}, \quad \boldsymbol{\xi}^{\mathrm{n}} = \begin{pmatrix} \mathbf{v}^{\mathrm{n}} \\ \mathbf{0} \end{pmatrix}, \mathbf{W}_{\boldsymbol{\xi}^{\mathrm{n}}} \triangleq \begin{pmatrix} \mathbf{0} \\ \mathbf{v}^{\mathrm{n}} \end{pmatrix}.$$

The advantage of taking local parameterization to be always about the current nominal twist $\boldsymbol{\xi}^{\mathrm{n}}$ is that $\boldsymbol{\eta}$ can be assumed to be infinitesimal to avoid differentiating a parameter-varying exponential map (see Section III-C).

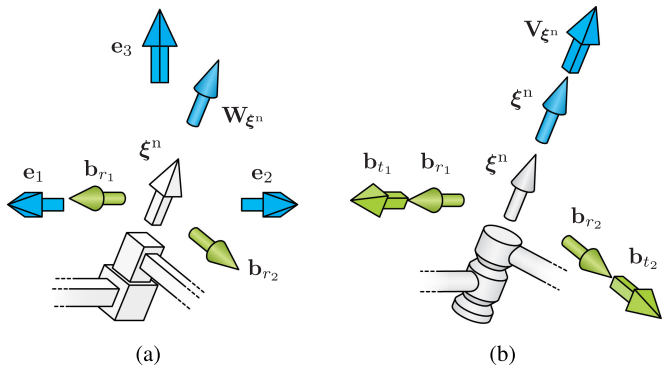

Fig. 6. Joint symmetries and calibration bases of (a) a prismatic joint and (b) a revolute joint.

In reference to (17) and (18), we may explicitly define the following matrix representation $\mathbf{B}$ for $\iota : \mathbb{R}^i \to \boldsymbol{\Sigma}_i, i = 4$ or 2:

$$\begin{aligned}\mathbf{B} &= \begin{pmatrix} \mathbf{b_{t_1}} & \mathbf{b}_{t_2} & \mathbf{b}_{r_1} & \mathbf{b}_{r_2} \end{pmatrix} \\ &= \begin{pmatrix} \mathbf{w_1} & \mathbf{w}_2 & \mathbf{q}^{\mathrm{n}} \times \mathbf{w}_1 & \mathbf{q}^{\mathrm{n}} \times \mathbf{w}_2 \\ \mathbf{0} & \mathbf{0} & \mathbf{w}_1 & \mathbf{w}_2 \end{pmatrix}_{6\times 4} \\ \mathbf{q}^{\mathrm{n}} &= \mathbf{w}^{\mathrm{n}} \times \mathbf{v}^{\mathrm{n}}, \qquad \boldsymbol{\xi}^{\mathrm{n}} = \begin{pmatrix} \mathbf{v}^{\mathrm{n}} \\ \mathbf{w}^{\mathrm{n}} \end{pmatrix}\end{aligned}$$

where $\mathbf{w}^{\mathrm{n}}$, $\mathbf{w}_1$, and $\mathbf{w}_2$ are mutually perpendicular unit vectors, $\mathbf{q}^{\mathrm{n}}$ is a point on the nominal joint axis; and

$$\mathbf{B} = \begin{pmatrix} \mathbf{b_{r_1}} & \mathbf{b}_{r_2} \end{pmatrix} = \begin{pmatrix} \mathbf{0} & \mathbf{0} \\ \mathbf{v}_1 & \mathbf{v}_2 \end{pmatrix}_{6\times 2}, \quad \boldsymbol{\xi}^{\mathrm{n}} = \begin{pmatrix} \mathbf{v}^{\mathrm{n}} \\ \mathbf{0} \end{pmatrix}$$

with $\mathbf{v}^{\mathrm{n}}$, $\mathbf{v}_1$, and $\mathbf{v}_2$ being also unit and mutually perpendicular. The span of columns of $\mathbf{B}$ gives the complement $\boldsymbol{\Sigma}_4$ of $\mathfrak{c}(\boldsymbol{\xi}^{\mathrm{n}})$ or $\boldsymbol{\Sigma}_2$ of $\mathfrak{r}(\boldsymbol{\xi}^{\mathrm{n}})$, as illustrated in Fig. 6, which satisfies (17) and (18) and therefore has eliminated parameterization redundancy. The Adjoint error (14) of the ith joint twist $\boldsymbol{\xi}_i$ can then be explicitly expressed as

$$\boldsymbol{\xi}_i^{\mathrm{a}} = \mathbf{Ad}_{e^{(\mathbf{B}\,\mathbf{k}_i)^\wedge}} \boldsymbol{\xi}_i^{\mathrm{n}}$$

where $\mathbf{k}_i$ is the corresponding minimal error parameter vector in the current step.

B. Error Model for the Tool Frame Offset

Since the error of the initial tool frame offset $\mathbf{g}_{st_0}$ can be any element $\mathbf{g} \in \mathbf{SE(3)}$, its error model may be given by the left action of $\mathbf{SE(3)}$ as

$$\Psi_{st} : \mathbf{SE(3)} \times \mathbf{SE(3)} \to \mathbf{SE(3)}, \quad (\mathbf{g}, \mathbf{g}_{st}) \mapsto \mathbf{g}\,\mathbf{g}_{st}.$$

The exponential map then gives a local parameterization of $\mathbf{g}_{st_0}$, as shown in Fig. 4(b) as

$$\exp : \mathbb{R}^6 \to \mathbf{SE}(3),\ \boldsymbol{\eta}_{st} \mapsto \mathbf{g}_{st_0}^{\mathrm{a}} = e^{\widehat{\boldsymbol{\eta}}_{st}} \mathbf{g}_{st_0}^{\mathrm{n}}. \tag{19}$$

Note that the above multiplicative parameterization is defined on a neighborhood of the current nominal offset $\mathbf{g}_{st_0}^{\mathrm{n}}$, which is implemented in [14] but not in [9], [13], and [20].

C. Linearized Adjoint Error Model

We adopt the same iterative linearization approach as in [9] during the identification process. The right pull back of the total differential of the kinematic function gives

$$\begin{aligned}\left((\delta \mathbf{g}_{st})\mathbf{g}_{st}^{-1}\right)^\vee = &\sum_{i=1}^{n} \mathbf{Ad}_{i-1} \left((\delta e^{\widehat{\boldsymbol{\xi}}_i \theta_i}) e^{-\widehat{\boldsymbol{\xi}}_i \theta_i}\right)^\vee \\ &+ \mathbf{Ad}_n \left((\delta \mathbf{g}_{st_0})\mathbf{g}_{st_0}^{-1}\right)^\vee \end{aligned} \tag{20}$$

in which we use the following notations:

$$\mathbf{Ad}_i \triangleq \mathbf{Ad}_{\prod_{j=1}^{i} e^{\widehat{\boldsymbol{\xi}}_j \theta_j}} = \prod_{j=1}^{i} \mathbf{Ad}_{e^{\widehat{\boldsymbol{\xi}}_j \theta_j}}, \quad \mathbf{Ad}_0 \triangleq \mathbf{I}$$

and $\vee$ is the inverse operation of $\wedge$. The linearization breaks down to calculating $((\delta e^{\widehat{\boldsymbol{\xi}}_i \theta_i}) e^{-\widehat{\boldsymbol{\xi}}_i \theta_i})^\vee$ and $((\delta \mathbf{g}_{st_0})\mathbf{g}_{st_0}^{-1})^\vee$.

According to our Adjoint error model (14), the twist error $((\delta e^{\widehat{\boldsymbol{\xi}}_i \theta_i}) e^{-\widehat{\boldsymbol{\xi}}_i \theta_i})^\vee$ of the ith joint is given by

$$\begin{aligned}&\left((\delta e^{\widehat{\boldsymbol{\xi}}_i \theta_i}) e^{-\widehat{\boldsymbol{\xi}}_i \theta_i}\right)^\vee \\ &= \left(\left(\delta \left(e^{\widehat{\boldsymbol{\eta}}_i} e^{\widehat{\boldsymbol{\xi}}_i^{\mathrm{n}} \theta_i} e^{-\widehat{\boldsymbol{\eta}}_i}\right)\right)\left(e^{\widehat{\boldsymbol{\eta}}_i} e^{\widehat{\boldsymbol{\xi}}_i^{\mathrm{n}} \theta_i} e^{-\widehat{\boldsymbol{\eta}}_i}\right)^{-1}\right)^\vee \\ &= \left(\mathbf{I} - \mathbf{Ad}_{e^{\widehat{\boldsymbol{\eta}}_i} e^{\widehat{\boldsymbol{\xi}}_i^{\mathrm{n}} \theta_i}}\right)\left((\delta e^{\widehat{\boldsymbol{\eta}}_i}) e^{-\widehat{\boldsymbol{\eta}}_i}\right)^\vee + \left(\mathbf{Ad}_{e^{\widehat{\boldsymbol{\eta}}_i}} \boldsymbol{\xi}_i^{\mathrm{n}}\right) \delta\theta_i \end{aligned} \tag{21}$$

where the nominal value $\boldsymbol{\xi}_i^{\mathrm{n}}$ is considered as a constant vector. Since $\boldsymbol{\eta}_i$ is a variable twist, $((\delta e^{\widehat{\boldsymbol{\eta}}_i}) e^{-\widehat{\boldsymbol{\eta}}_i})^\vee$ is given by the differentiation of a parameter-varying matrix exponential [9]:

$$\left((\delta e^{\widehat{\boldsymbol{\eta}}_i}) e^{-\widehat{\boldsymbol{\eta}}_i}\right)^\vee = \left(\int_0^1 \mathbf{Ad}_{e^{\widehat{\boldsymbol{\eta}}_i s}} \mathrm{d}s\right) \delta\boldsymbol{\eta}_i.$$

Although the above equation has a closed-form expression, it is much slower to compute than Adjoint transformations and exponential maps [10]. As we will see in Section VI-B, it substantially increases the running time of several POE-based calibration algorithms.

Since in each iteration, the Adjoint error model always parameterizes $\mathscr{C}_{\mathcal{R}}$ or $\mathscr{C}_{\mathcal{P}}$ on a neighborhood of the current nominal twist $\boldsymbol{\xi}_{\mathrm{i}}^{\mathrm{n}}$, we always have $\boldsymbol{\eta}_i = 0$. Equation (21) can then be simplified to

$$\left((\delta e^{\widehat{\boldsymbol{\xi}}_i \theta_i}) e^{-\widehat{\boldsymbol{\xi}}_i \theta_i}\right)^\vee = \left(\mathbf{I} - \mathbf{Ad}_{e^{\widehat{\boldsymbol{\xi}}_i^{\mathrm{n}} \theta_i}}\right) \delta\boldsymbol{\eta}_i + \boldsymbol{\xi}_i^{\mathrm{n}} \delta\theta_i \tag{22}$$

without differentiating the parameter-varying exponential map.

Linearization of the initial tool frame offset error can be derived in a similar manner as

$$\begin{aligned}\left((\delta \mathbf{g}_{st_0})\mathbf{g}_{st_0}^{-1}\right)^\vee &= \left(\left(\delta \left(e^{\widehat{\boldsymbol{\eta}}_{st}} \mathbf{g}_{st_0}^{\mathrm{n}}\right)\right)\left(e^{\widehat{\boldsymbol{\eta}}_{st}} \mathbf{g}_{st_0}^{\mathrm{n}}\right)^{-1}\right)^\vee \\ &= \left((\delta e^{\widehat{\boldsymbol{\eta}}_{st}}) e^{-\widehat{\boldsymbol{\eta}}_{st}}\right)^\vee = \delta\boldsymbol{\eta}_{st}. \end{aligned} \tag{23}$$

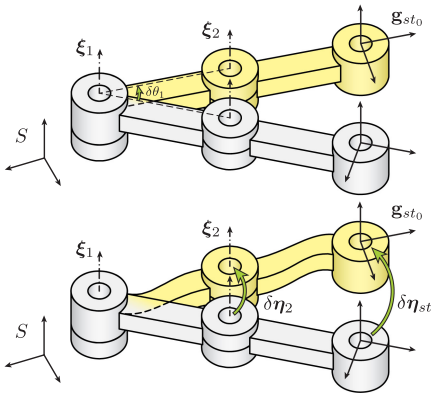

Fig. 7. Same end-effector error caused by encoder offset or Adjoint errors.

Substitute (22) and (23) into (20) and we have

$$\left((\delta\mathbf{g}_{st})\mathbf{g}_{st}^{-1}\right)^{\vee} = \sum_{i=1}^{n}(\mathbf{Ad}_{i-1} - \mathbf{Ad}_i)\delta\boldsymbol{\eta}_i + \sum_{i=1}^{n}\left(\mathbf{Ad}_{i-1}\boldsymbol{\xi}_i^{\mathrm{n}}\right)\delta\theta_i + \mathbf{Ad}_n\delta\boldsymbol{\eta}_{st}. \quad (24)$$

It is proved that the joint encoder offsets and the Adjoint errors cannot be simultaneously identified [10]–[12]. Physically it means the end-effector error caused by encoder offsets may be attributed to equivalent Adjoint errors (but in general not vice versa), as illustrated in Fig. 7. Therefore, all the joint encoder offsets $\delta\theta_i$ may be simply ignored without losing completeness. The matrix form of (24) is given by

$$\left((\delta\mathbf{g}_{st})\mathbf{g}_{st}^{-1}\right)^{\vee} = \underbrace{\begin{pmatrix}\mathbf{Q_1} & \cdots & \mathbf{Q}_n & \mathbf{Q}_{st}\end{pmatrix}\mathbb{B}}_{\mathbf{A}}\mathbf{k} \quad (25)$$

where

$$\mathbf{Q}_i = \mathbf{Ad}_{i-1} - \mathbf{Ad}_i,\ \mathbf{Q}_{st} = \mathbf{Ad}_n,\ \delta\boldsymbol{\eta}_i = \mathbf{B}_i\mathbf{k}_i,\ \delta\boldsymbol{\eta}_{st} = \mathbf{E}_{st}\mathbf{k}_{st}$$

$$\mathbb{B} = \begin{pmatrix}\mathbf{B_1} & \cdots & \mathbf{0} & \mathbf{0}\\ \vdots & \ddots & \vdots & \mathbf{0}\\ \mathbf{0} & \cdots & \mathbf{B}_n & \mathbf{0}\\ \mathbf{0} & \cdots & \mathbf{0} & \mathbf{E}_{st}\end{pmatrix},\ \mathbf{k} = \begin{pmatrix}\mathbf{k_1}\\ \vdots\\ \mathbf{k}_n\\ \mathbf{k}_{st}\end{pmatrix}.$$

$\mathbf{k}$ contains the minimal error parameters for each joint twists $\mathbf{k}_i$ and initial tool frame offset $\mathbf{k}_{st}$. The expression for $\mathbf{E}_{st}$ and $\mathbf{k}_{st}$ depends on the type of measurement.

D. Calibration With Pose and Point Measurements

1) Pose Measurements: If the tool frame pose $\mathbf{g}_{st}^{\mathrm{a}}$ is measured, the infinitesimal pose error can be approximated by

$$\mathbf{y} = \left((\delta\mathbf{g}_{st})\mathbf{g}_{st}^{-1}\right)^{\vee} \approx \log\left(\mathbf{g}_{st}^{\mathrm{a}}(\mathbf{g}_{st}^{\mathrm{n}})^{-1}\right)$$

and (25) is defined with $\mathbf{E}_{st} = \mathbf{I}_{6\times 6}$ and $\mathbf{k}_{st} \in \mathbb{R}^6$; $\mathbf{k}$ is a vector in $\mathbb{R}^{4r+2t+6}$. Given m end-effector pose measurements $\mathbf{y}^i$ and corresponding Jacobian matrix $\mathbf{A}^i$, $i = 1, \ldots, m$, the overall error equation is given by

$$\mathbf{Y} = \begin{pmatrix}\mathbf{y^1}\\ \vdots\\ \mathbf{y}^m\end{pmatrix} = \begin{pmatrix}\mathbf{A^1}\\ \vdots\\ \mathbf{A}^m\end{pmatrix}\mathbf{k} = \mathbb{A}\mathbf{k}.$$

$\mathbf{k}$ is identifiable if all columns of the calibration Jacobian matrix $\mathbb{A}$ are linearly independent. This is true only if $6m \geq 4r + 2t + 6$. We have the following theorem.

Theorem 1: There exists a sampling strategy with $r + t + 1$ pose measurements under which all the $4r + 2t + 6$ parameters in $\mathbf{k}$ are identifiable. ♢

The sampling strategy in the proof (see Appendix B) is only chosen for proving the identifiability. In practice, more than $r + t + 1$ poses are sampled to counter the measurement noise. We emphasize that the above lower bound on the number of measurements is not tight, but low enough for, for example, analytical study of observability index [31], [32]. The derivation of a tight lower bound using screw theory is possible, but is much involved and therefore omitted.

2) Point Measurements: Without loss of generality, we let the measure point be the tool frame origin, whose coordinates in the spatial frame S are $\tilde{\mathbf{q}}_e = \mathbf{g}_{st}\cdot(0,0,0,1)^{\mathrm{T}}$. The infinitesimal point error is given by

$$\delta\tilde{\mathbf{q}}_e = (\delta\mathbf{g}_{st})\,\mathbf{g}_{st}^{-1}\,\mathbf{g}_{st}\begin{pmatrix}0 & 0 & 0 & 1\end{pmatrix}^{\mathrm{T}} = ((\delta\mathbf{g}_{st})\mathbf{g}_{st}^{-1})\tilde{\mathbf{q}}_e^{\mathrm{n}}.$$

Consequently, we have [11]

$$\mathbf{y} = \mathbf{q}_e^{\mathrm{a}} - \mathbf{q}_e^{\mathrm{n}} \approx \delta\mathbf{q}_e = \begin{pmatrix}\mathbf{I} & -\widehat{\mathbf{q}}_e^{\mathrm{n}}\end{pmatrix}\left((\delta\mathbf{g}_{st})\mathbf{g}_{st}^{-1}\right)^{\vee} = \underbrace{\begin{pmatrix}\mathbf{I} & -\widehat{\mathbf{q}}_e^{\mathrm{n}}\end{pmatrix}\begin{pmatrix}\mathbf{Q_1} & \cdots & \mathbf{Q}_n & \mathbf{Q}_{st}\end{pmatrix}\mathbb{B}}_{\mathbf{A}}\mathbf{k} \quad (26)$$

with

$$\mathbf{E}_{st} = \begin{pmatrix}\mathbf{I}_{3\times 3}\\ \mathbf{0}_{3\times 3}\end{pmatrix},\ \mathbf{k}_{st} = \delta\mathbf{q}_{e_0},\ \mathbf{q}_{e_0} \triangleq \mathbf{g}_{st_0}(0,0,0,1)^{\mathrm{T}}. \quad (27)$$

In this case, $\mathbf{k} \in \mathbb{R}^{4r+2t+3}$ instead of $\mathbb{R}^{4r+2t+6}$ since we cannot recover the initial tool frame orientation from point measurements (see Appendix C). In order to fulfill the full column rank condition for $\mathbb{A}$, the number of measurements should satisfy $3m \geq 4r + 2t + 3$. We have the following theorem (see Appendix C for proof):

Theorem 2: There exists a sampling strategy with $2r + t + 1$ point measurements under which all the $4r + 2t + 3$ parameters in $\mathbf{k}$ are identifiable. In particular, if the last joint is a revolute joint, the measurement point must not lie on its axis. ♢

If the last s joints are all revolute joints and the measurement point lies on their axes, we have $2s$ less identifiable parameters corresponding to the rotations of the last s joints about point $\mathbf{q}_{e_0}$ (see also Appendix C). Note that this corroborates the same conclusion in [33]. The case for $s = 1$ is shown in Fig. 8, where $\delta\boldsymbol{\eta}_r$ of the last joint cannot be calibrated.

With a sampling strategy satisfying the full column rank condition of $\mathbb{A}$, the least square solution of the error parameter $\mathbf{k}$ in the current iteration is given by

$$\mathbf{k} = \mathbb{A}^{\dagger}\mathbf{Y} = (\mathbb{A}^{\mathrm{T}}\mathbb{A})^{-1}\mathbb{A}^{\mathrm{T}}\mathbf{Y}. \quad (28)$$

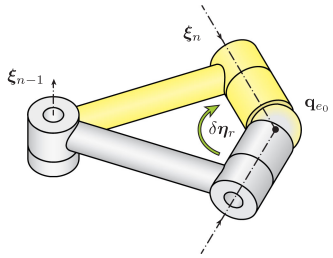

Fig. 8. Rotation of the last joint cannot be identified.

1: Describe robot nominal model $\boldsymbol{\xi}_i^{\mathrm{n}}, \mathbf{g}_{st_0}^{\mathrm{n}}$
2: Take multiple samples and measure the tool frame poses/positions
3: **repeat**
4: Identify $\mathbf{k} = \mathbb{A}^{\dagger}\mathbf{Y}$ using (28)
5: Update parameters $\boldsymbol{\xi}_i^{\mathrm{a}}, \mathbf{g}_{st_0}^{\mathrm{a}}$ using (29)
6: **until** $\|\mathbf{k}\| < \epsilon$

Fig. 9. Calibration procedure using Adjoint error model.

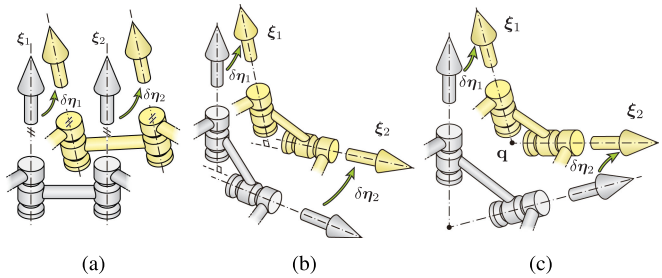

Fig. 10. Two joint axes keep (a) parallel, (b) perpendicular, and (c) concurrent.

Multiplicative error updates (14) and (19) are then applied to generate $\boldsymbol{\xi}_i^{\mathrm{a}}$'s and $\mathbf{g}_{st_0}^{\mathrm{a}}$ using the identified parameters $\mathbf{k}$ as

$$\begin{cases} \boldsymbol{\xi}_i^{\mathrm{a}} = \mathbf{Ad}_{e^{\delta\hat{\boldsymbol{\eta}}_i}}\boldsymbol{\xi}_i^{\mathrm{n}}, \quad \delta\boldsymbol{\eta}_i = \mathbf{B}_i\mathbf{k}_i,\ i = 1,\ldots,n \\ \mathbf{g}_{st_0}^{\mathrm{a}} = e^{\widehat{\mathbf{k}}_{st}}\mathbf{g}_{st_0}^{\mathrm{n}}. \end{cases} \tag{29}$$

The linearized calibration process is then iterated with $\boldsymbol{\xi}_i^{\mathrm{a}}$'s and $\mathbf{g}_{st_0}^{\mathrm{a}}$ being the new nominal values until convergence is reached. The calibration procedure is summarized in Fig. 9.

IV. Assumptions on Joint Axes Geometry

Most commercial control systems have implicit geometric assumptions on the joint relations. In particular, neighboring joint axes are usually assumed perpendicular, parallel, or concurrent. Since such assumptions are not subject to user modification, the pose redefinition method [34] is often adopted with an external PC, which inevitably limits the robot controller's performance. Besides, some of the assumptions in fact reflect certain physical features of the robot. For instance, the last two joints of a SCARA robot should be parallel when they share the same ball-screw-spline unit. Under such circumstances, it is reasonable to maintain the feasibility of constraints satisfied during calibration. Typical constraints are illustrated in Fig. 10, which can be easily maintained by modifying the basis matrix $\mathbf{B}$ in the Adjoint error model.

A. Two Consecutive Joint Axes Being Parallel

If two neighboring joint twists $\boldsymbol{\xi}_i^{\mathrm{n}}, \boldsymbol{\xi}_{i+1}^{\mathrm{n}}$ are assumed to be parallel, their basis matrices $\mathbf{B}_i, \mathbf{B}_{i+1}$ should share the same rotational bases while having different translational bases

$$\mathbf{B}_{i,i+1} = \begin{pmatrix} \mathbf{b}_{i,r_1} & \mathbf{b}_{i,r_2} & \mathbf{b}_{i,t_1} & \mathbf{b}_{i,t_2} & \mathbf{0} & \mathbf{0} \\ \mathbf{b}_{i,r_1} & \mathbf{b}_{i,r_2} & \mathbf{0} & \mathbf{0} & \mathbf{b}_{i+1,t_1} & \mathbf{b}_{i+1,t_2} \end{pmatrix}_{12\times 6}. \tag{30}$$

In particular, if $\boldsymbol{\xi}_i^{\mathrm{n}}$ is a prismatic twist, (30) reduces to

$$\mathbf{B}_{i,i+1} = \begin{pmatrix} \mathbf{b}_{i,r_1} & \mathbf{b}_{i,r_2} & \mathbf{0} & \mathbf{0} \\ \mathbf{b}_{i,r_1} & \mathbf{b}_{i,r_2} & \mathbf{b}_{i+1,t_1} & \mathbf{b}_{i+1,t_2} \end{pmatrix}_{12\times 4}$$

which is the case for the last two joints of a SCARA robot.

B. Two Consecutive Joint Axes Being Perpendicular

Besides the same rotational basis, $\boldsymbol{\xi}_{i+1}^{\mathrm{n}}$ can rotate about the revolute joint $\boldsymbol{\xi}_i^{\mathrm{n}}$ while remaining perpendicular to it as

$$\mathbf{B}_{i,i+1} = \begin{pmatrix} \mathbf{b}_{i,r_1} & \mathbf{b}_{i,r_2} & \mathbf{b}_{i,t_1} & \mathbf{b}_{i,t_2} & \mathbf{0} & \mathbf{0} & \mathbf{0} \\ \mathbf{b}_{i,r_1} & \mathbf{b}_{i,r_2} & \mathbf{0} & \mathbf{0} & \mathbf{b}_{i+1,t_1} & \mathbf{b}_{i+1,t_2} & \boldsymbol{\xi}_i^{\mathrm{n}} \end{pmatrix}_{12\times 7}.$$

This additional degree of freedom can also be viewed as a joint encoder offset $\delta\theta_i$. The error update of $\boldsymbol{\xi}_{i+1}$ becomes

$$\boldsymbol{\xi}_{i+1}^{\mathrm{a}} = \mathbf{Ad}_{e^{\left(\sum_{j=1}^{6} k_j \mathbf{b}_j\right)^{\wedge}} e^{k_7 \widehat{\boldsymbol{\xi}}_i^{\mathrm{n}}}} \boldsymbol{\xi}_{i+1}^{\mathrm{n}}$$

where k_j is the jth component of error vector $\mathbf{k}_{i,i+1}$, and $\mathbf{b}_j$ is the corresponding basis vector at the jth column of $\mathbf{B}_{i,i+1}$. When joint i is a prismatic one, the basis matrix becomes

$$\mathbf{B}_{i,i+1} = \begin{pmatrix} \mathbf{0} & \mathbf{b}_{i,r_1} & \mathbf{b}_{i,r_2} & \mathbf{0} & \mathbf{0} \\ \mathbf{W}_{\boldsymbol{\xi}_i^{\mathrm{n}}} & \mathbf{b}_{i,r_1} & \mathbf{b}_{i,r_2} & \mathbf{b}_{i+1,t_1} & \mathbf{b}_{i+1,t_2} \end{pmatrix}_{12\times 5}.$$

C. Two Consecutive Joint Axes Being Concurrent

When the axes of $\boldsymbol{\xi}_i^{\mathrm{n}}, \boldsymbol{\xi}_{i+1}^{\mathrm{n}}$ are assumed to be concurrent, they can rotate about the intersection point and translate together as

$$\mathbf{B}_{i,i+1} = \begin{pmatrix} \mathbf{b_{i,r_1}} & \mathbf{b}_{i,r_2} & \mathbf{0} & \mathbf{0} & \mathbf{e}_1 & \mathbf{e}_2 & \mathbf{e}_3 \\ \mathbf{0} & \mathbf{0} & \mathbf{b}_{i+1,r_1} & \mathbf{b}_{i+1,r_2} & \mathbf{e}_1 & \mathbf{e}_2 & \mathbf{e}_3 \end{pmatrix}_{12\times 7}$$

$$\boldsymbol{\xi}_i^{\mathrm{a}} = \mathbf{Ad}_{e^{\left(\sum_{j=1}^{3} k_{j+4}\mathbf{e}_j\right)^{\wedge}} e^{\left(k_1 \mathbf{b}_{i,r_1} + k_2 \mathbf{b}_{i,r_2}\right)^{\wedge}}} \boldsymbol{\xi}_i^{\mathrm{n}}$$

$$\boldsymbol{\xi}_{i+1}^{\mathrm{a}} = \mathbf{Ad}_{e^{\left(\sum_{j=1}^{3} k_{j+4}\mathbf{e}_j\right)^{\wedge}} e^{\left(k_3 \mathbf{b}_{i+1,r_1} + k_4 \mathbf{b}_{i+1,r_2}\right)^{\wedge}}} \boldsymbol{\xi}_{i+1}^{\mathrm{n}}.$$

If we assign one of $\mathbf{b}_{i+1,r_1}, \mathbf{b}_{i+1,r_2}$ to be $\boldsymbol{\xi}_i^{\mathrm{n}}$, the amount of change can be interpreted as a joint encoder offset $\delta\theta_i$.

We can combine the above three basic assumptions for more complicated scenarios. Note that we take advantage of the fact that $\mathbf{b}_{t_1}, \mathbf{b}_{t_2}$ and $\mathbf{b}_{r_1}, \mathbf{b}_{r_2}$ are purely translational and rotational changes, respectively. In comparison, the orthonormal basis in [20] can effectively remove parameter redundancy as well, but is hard to impose additional assumptions on joint axes relations with its Gram–Schmidt procedure.

V. Comparative Study of Error Models and Calibration Algorithms

The geometric ACS model and Adjoint error framework of our algorithm can be used to reflect upon existing error models and calibration algorithms in a unified manner.

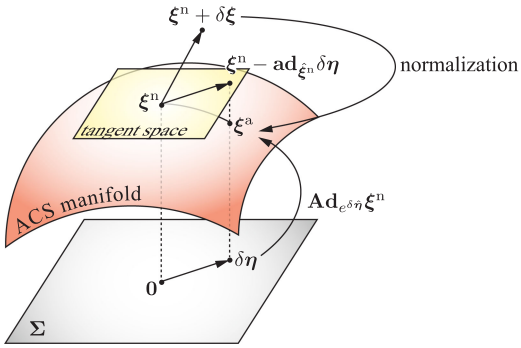

Fig. 11. Relation between additive error and multiplicative error.

A. Additive Error Versus Multiplicative Error

Adjoint error is a multiplicative error, which should be distinguished from an additive error model as

$$\boldsymbol{\xi}^{\mathrm{a}} = \boldsymbol{\xi}^{\mathrm{n}} + \delta\boldsymbol{\xi}.$$

It can be proved (see Appendix D) that, in the case of a revolute joint for instance, when $\delta\boldsymbol{\xi} \in \mathfrak{c}(\boldsymbol{\xi}^{\mathrm{n}})$, the additive error update in the standard POE model [9] takes no effect after normalization. Consequently, a complementary subspace $\boldsymbol{\Sigma}_4$ of $\mathfrak{c}(\boldsymbol{\xi}^{\mathrm{n}})$ in $\mathbf{se(3)}$ defines a parameterization of the ACS manifold $\mathbf{T}(\mathbf{S}^2)$ after normalization as

$$\begin{aligned} &\boldsymbol{\Sigma}_4 \to \mathbf{T}(\mathbf{S}^2), \quad \delta\boldsymbol{\xi} \mapsto \boldsymbol{\xi}^{\mathrm{n}} + \delta\boldsymbol{\xi} \\ &\boldsymbol{\Sigma}_4 \oplus \mathfrak{c}(\boldsymbol{\xi}^{\mathrm{n}}) = \mathbf{se(3)}. \end{aligned} \tag{31}$$

On the other hand, an infinitesimal Adjoint error is equivalent to a particular additive error using the adjoint map[3] $\mathbf{ad}_{\hat{\boldsymbol{\eta}}}$ as

$$\boldsymbol{\xi}^{\mathrm{a}} = \mathbf{Ad}_{e^{\hat{\boldsymbol{\eta}}}}\boldsymbol{\xi}^{\mathrm{n}} = e^{\mathbf{ad}_{\hat{\boldsymbol{\eta}}}}\boldsymbol{\xi}^{\mathrm{n}} \approx (\mathbf{I} + \mathbf{ad}_{\hat{\boldsymbol{\eta}}})\boldsymbol{\xi}^{\mathrm{n}} = \boldsymbol{\xi}^{\mathrm{n}} \underbrace{- \mathbf{ad}_{\hat{\boldsymbol{\xi}}^{\mathrm{n}}}\boldsymbol{\eta}}_{\delta\boldsymbol{\xi}}. \tag{32}$$

In reference to (31) and the fact that $\ker(\mathbf{ad}_{\hat{\boldsymbol{\xi}}^{\mathrm{n}}}) = \mathfrak{c}(\boldsymbol{\xi}^{\mathrm{n}})$, $\mathrm{Im}(\mathbf{ad}_{\hat{\boldsymbol{\xi}}^{\mathrm{n}}}) \oplus \mathfrak{c}(\boldsymbol{\xi}^{\mathrm{n}}) = \mathbf{se(3)}$, $\boldsymbol{\xi}^{\mathrm{n}} \in \mathbf{T}(\mathbf{S}^2)$, we may have the following parameterization for $\mathbf{T}(\mathbf{S}^2)$ as

$$\boldsymbol{\Sigma}_4 \to \mathbf{T}(\mathbf{S}^2), \quad \boldsymbol{\eta} \mapsto \boldsymbol{\xi}^{\mathrm{n}} \underbrace{- \mathbf{ad}_{\hat{\boldsymbol{\xi}}^{\mathrm{n}}}\boldsymbol{\eta}}_{\delta\boldsymbol{\xi}} \tag{33}$$

which is a linearization of (16). $\delta\boldsymbol{\xi}$ takes value in $\mathrm{Im}(\mathbf{ad}_{\hat{\boldsymbol{\xi}}^{\mathrm{n}}})$, the tangent space $\mathbf{T}_{\boldsymbol{\xi}^{\mathrm{n}}}[\mathbf{T}(\mathbf{S}^2)]$ of $\mathbf{T}(\mathbf{S}^2)$ at $\boldsymbol{\xi}^{\mathrm{n}}$.

It should be pointed out that neither (31) nor (33) respect the nonlinear geometry of $\mathbf{T}(\mathbf{S}^2)$ and must work with a normalization process (see Fig. 11). Besides, the additive error update introduces the costly differentiation operation of parameter-varying matrix exponentials, which is presented in the standard POE model [9], the minimal POE model [13], and the RLPOE model [20] (see Table I).

B. Kinematic and Error Models

In our calibration algorithm, we distinguish the space of twist coordinates $\boldsymbol{\xi}$ from that of their errors $\boldsymbol{\eta}$ so that the geometry of the ACS manifolds are not violated during error update (see Fig. 11). This is not the case with the DH or standard POE approaches, where the DH parameters or the joint twists are used as both kinematic and error parameters. The minimal POE algorithm implements a refined additive error update, and the local POE and RLPOE adopt the dyad kinematics model. Their kinematic models and error update schemes are summarized in Table I.

1) DH Approach: Transformation between local frames in the DH approach can be essentially represented by the product of four exponentials [10] as

$$\mathbf{g}_{i,i+1} = e^{\hat{\mathbf{e}}_6\theta_i} e^{\hat{\mathbf{e}}_3 d_i} e^{\hat{\mathbf{e}}_4\alpha_i} e^{\hat{\mathbf{e}}_1 a_i} = e^{\hat{\mathbf{e}}_6\theta_i + \hat{\mathbf{e}}_3 d_i} e^{\hat{\mathbf{e}}_4\alpha_i + \hat{\mathbf{e}}_1 a_i}.$$

The relative location of $\boldsymbol{\xi}^{\mathrm{n}}_{i+1}$ (assuming, without loss of generality, a revolute joint) with respect to the local frame i is given by

$$\boldsymbol{\xi}^{\mathrm{n}}_{i,i+1} = \mathbf{Ad}_{e^{\hat{\mathbf{e}}_6\theta_i + \hat{\mathbf{e}}_3 d_i} e^{\hat{\mathbf{e}}_4\alpha_i + \hat{\mathbf{e}}_1 a_i}} \mathbf{e}_6$$

and the DH parameter error $(\delta\theta_i, \delta d_i, \delta\alpha_i, \delta a_i)$ parameterizes the ACS manifold of $\boldsymbol{\xi}_{i+1}$ by

$$\begin{aligned} &\mathbb{R}^4 \to \mathbf{T}(\mathbf{S}^2) \\ &(\delta\theta_i, \delta d_i, \delta\alpha_i, \delta a_i) \mapsto \mathbf{Ad}_{e^{\hat{\mathbf{e}}_6\delta\theta_i + \hat{\mathbf{e}}_3\delta d_i} e^{\hat{\mathbf{e}}'_4\delta\alpha_i + \hat{\mathbf{e}}'_1\delta a_i}} \boldsymbol{\xi}^{\mathrm{n}}_{i,i+1} \end{aligned}$$

with $\mathbf{e}'_4 = \mathbf{Ad}_{e^{\hat{\mathbf{e}}_6\theta_i + \hat{\mathbf{e}}_3 d_i}}\mathbf{e}_4$ and $\mathbf{e}'_1 = \mathbf{Ad}_{e^{\hat{\mathbf{e}}_6\theta_i + \hat{\mathbf{e}}_3 d_i}}\mathbf{e}_1$, as in Fig. 12(a). In other words, the DH parameter space is the 4-D product manifold $\mathbf{C}(\mathbf{e}_6) \times \mathbf{C}(\mathbf{e}'_4)$, which is topologically distinct from the ACS manifold $\mathbf{T}(\mathbf{S}^2)$. Therefore, the model discontinuity is inevitable: in reference to the direct sum condition (17), $\mathbf{e}_6, \mathbf{e}_3, \mathbf{e}'_4, \mathbf{e}'_1$ fail to span a complementary subspace of $\mathfrak{c}(\boldsymbol{\xi}^{\mathrm{n}}_{i,i+1})$ in $\mathbf{se(3)}$ when $\alpha_i = 0$, as in Fig. 12(b).

2) Standard POE Model: The standard POE approach implements an arbitrary additive error $\delta\boldsymbol{\xi} \in \mathbf{se(3)}$ on the joint twist coordinates as in Fig. 12(c). By the linearized Adjoint error $\delta\boldsymbol{\xi} \approx -\mathbf{ad}_{\hat{\boldsymbol{\xi}}}\delta\boldsymbol{\eta}$ illustrated in (32) and the chain rule [11] as

$$((\delta e^{\hat{\boldsymbol{\xi}}\theta})e^{-\hat{\boldsymbol{\xi}}\theta})^{\vee} = -\theta\left(\int_0^1 \mathbf{Ad}_{e^{\hat{\boldsymbol{\xi}}\theta s}}\mathrm{d}s\right)\mathbf{ad}_{\hat{\boldsymbol{\xi}}}\delta\boldsymbol{\eta} + \boldsymbol{\xi}\delta\theta$$

which leads to the Adjoint error model (22) after full simplification [10] (the full simplification was not carried out in our earlier work [11]).

3) Minimal POE Model: The minimal POE model [13] localizes the nominal twist to always coincide with the local $\mathbf{z}$-axis, and parameterizes the actual axis with a point $\mathbf{p}^{\mathrm{a}}_i = (p_{\mathbf{x}}, p_{\mathbf{y}}, 0)^{\mathrm{T}}$ and a direction deviation in the $\mathbf{xy}$-components $w_{\mathbf{x}}$ and $w_{\mathbf{y}}$, as in Fig. 12(d). Its error update is equivalent to the

[3]The adjoint map $\mathbf{ad}_{\hat{\boldsymbol{\xi}}} : \mathbf{se(3)} \to \mathbf{se(3)}$ with $\boldsymbol{\xi} \in \mathbf{se(3)}$ is defined by $(\mathbf{ad}_{\hat{\boldsymbol{\xi}}}\boldsymbol{\zeta})^{\wedge} \triangleq \hat{\boldsymbol{\xi}}\hat{\boldsymbol{\zeta}} - \hat{\boldsymbol{\zeta}}\hat{\boldsymbol{\xi}}, \forall\boldsymbol{\zeta} \in \mathbf{se(3)}$ and is equal to the Lie bracket $[\hat{\boldsymbol{\xi}}, \hat{\boldsymbol{\zeta}}]$ [8]. $\mathbf{ad}_{\hat{\boldsymbol{\xi}}}$ is a linear map with matrix representation as

$$\mathbf{ad}_{\hat{\boldsymbol{\xi}}} = \begin{pmatrix} \hat{\mathbf{w}} & \hat{\mathbf{v}} \\ \mathbf{0}_{3\times 3} & \hat{\mathbf{w}} \end{pmatrix} \in \mathbb{R}^{6\times 6}, \quad \boldsymbol{\xi} = \begin{pmatrix} \mathbf{v} \\ \mathbf{w} \end{pmatrix}.$$

See, for example, [22, Proposition 2.25] for the relation $\mathbf{Ad}_{e^{\hat{\boldsymbol{\eta}}}} = e^{\mathbf{ad}_{\hat{\boldsymbol{\eta}}}}$.

TABLE I
SUMMARY OF KINEMATIC AND ERROR MODELS

Method	Kinematic model	Error model	Linearization of a single joint
DH	$\mathbf{g}_{st} = \prod_{i=0}^{n+1} \mathrm{R}_{\mathbf{z}}(\theta_i)\mathrm{T}_{\mathbf{z}}(d_i)\mathrm{R}_{\mathbf{x}}(\alpha_i)\mathrm{T}_{\mathbf{x}}(a_i)$ $= \prod_{i=0}^{n+1} e^{\widehat{\mathbf{e}}_6\theta_i} e^{\widehat{\mathbf{e}}_3 d_i} e^{\widehat{\mathbf{e}}_4\alpha_i} e^{\widehat{\mathbf{e}}_1 a_i}$	$\theta_i^{\mathrm{a}} = \theta_i^{\mathrm{n}} + \delta\theta_i;\quad d_i^{\mathrm{a}} = d_i^{\mathrm{n}} + \delta d_i$ $\alpha_i^{\mathrm{a}} = \alpha_i^{\mathrm{n}} + \delta\alpha_i;\quad a_i^{\mathrm{a}} = a_i^{\mathrm{n}} + \delta a_i$	$\left(\delta\mathbf{g}_{i,i+1}\mathbf{g}_{i,i+1}^{-1}\right)^{\vee} = \mathbf{e}_6\delta\theta_i + \mathbf{e}_3\delta d_i$ $+ \mathbf{Ad}_{e^{\widehat{\mathbf{e}}_6\theta_i}} + \mathbf{Ad}_{e^{\widehat{\mathbf{e}}_3 d_i}}(\mathbf{e}_1\delta a_i + \mathbf{e}_4\delta\alpha_i)$
Standard POE	$\mathbf{g}_{st} = e^{\widehat{\boldsymbol{\xi}}_1\theta_1} e^{\widehat{\boldsymbol{\xi}}_2\theta_2} \cdots e^{\widehat{\boldsymbol{\xi}}_n\theta_n} e^{\widehat{\boldsymbol{\xi}}_{st}}$	$\boldsymbol{\xi}_i^{\mathrm{a}} = \boldsymbol{\xi}_i^{\mathrm{n}} + \delta\boldsymbol{\xi}_i;\ \theta_i^{\mathrm{a}} = \theta_i^{\mathrm{n}} + \delta\theta_i$ $\boldsymbol{\xi}_{st}^{\mathrm{a}} = \boldsymbol{\xi}_{st}^{\mathrm{n}} + \delta\boldsymbol{\xi}_{st}$	$\left(\delta e^{\widehat{\boldsymbol{\xi}}_i\theta_i} e^{-\widehat{\boldsymbol{\xi}}_i\theta_i}\right)^{\vee} = \theta_i\int_0^1 \mathbf{Ad}_{e^{\widehat{\boldsymbol{\xi}}_i\theta_i s}}\mathrm{d}s\cdot\delta\boldsymbol{\xi}_i + \boldsymbol{\xi}_i\delta\theta_i$
Minimal POE	$\mathbf{g}_{st} = e^{\widehat{\boldsymbol{\xi}}_1\theta_1} e^{\widehat{\boldsymbol{\xi}}_2\theta_2} \cdots e^{\widehat{\boldsymbol{\xi}}_n\theta_n} e^{\widehat{\boldsymbol{\xi}}_{st}}$	$\boldsymbol{\xi}_i^{\mathrm{a}} = \mathbf{Ad}_{\mathbf{g}_i}\boldsymbol{\xi}_i'(\boldsymbol{\sigma}_i^{\mathrm{n}} + \delta\boldsymbol{\sigma}_i)$ $\theta_i^{\mathrm{a}} = \theta_i^{\mathrm{n}} + \delta\theta_i;\ \boldsymbol{\xi}_{st}^{\mathrm{a}} = \boldsymbol{\xi}_{st}^{\mathrm{n}} + \delta\boldsymbol{\xi}_{st}$	$\left(\delta e^{\widehat{\boldsymbol{\xi}}_i\theta_i} e^{-\widehat{\boldsymbol{\xi}}_i\theta_i}\right)^{\vee} = \theta_i\int_0^1 \mathbf{Ad}_{e^{\widehat{\boldsymbol{\xi}}_i\theta_i s}}\mathrm{d}s\,\frac{\partial\boldsymbol{\xi}_i}{\partial\boldsymbol{\sigma}_i}\delta\boldsymbol{\sigma}_i + \boldsymbol{\xi}_i\delta\theta_i$
Local POE	$\mathbf{g}_{st} = e^{\widehat{\mathbf{p}}_1} e^{\widehat{s}_1\theta_1} \cdots e^{\widehat{\mathbf{p}}_n} e^{\widehat{s}_n\theta_n} e^{\widehat{\mathbf{p}}_{n+1}}$	$e^{\widehat{\mathbf{p}}_i^{\mathrm{a}}} = e^{\delta\widehat{\mathbf{p}}_i} e^{\widehat{\mathbf{p}}_i^{\mathrm{n}}}$	$(\delta\mathbf{g}_{i-1,i}\mathbf{g}_{i-1,i}^{-1})^{\vee} = \delta\mathbf{p}_i$
RLPOE	$\mathbf{g}_{st} = e^{\widehat{\mathbf{p}}_1} e^{\widehat{s}_1\theta_1} \cdots e^{\widehat{\mathbf{p}}_n} e^{\widehat{s}_n\theta_n} e^{\widehat{\mathbf{p}}_{n+1}}$	$\widehat{\mathbf{p}}_i^{\mathrm{a}} = \widehat{\mathbf{p}}_i^{\mathrm{n}} + \delta_{\widehat{\mathbf{p}}_i}$	$(\delta\mathbf{g}_{i-1,i}\mathbf{g}_{i-1,i}^{-1})^{\vee} = \int_0^1 \mathbf{Ad}_{e^{\widehat{\mathbf{p}}_i s}}\mathrm{d}s\cdot\delta\mathbf{p}_i$
Adjoint Error	$\mathbf{g}_{st} = e^{\widehat{\boldsymbol{\xi}}_1\theta_1} e^{\widehat{\boldsymbol{\xi}}_2\theta_2} \cdots e^{\widehat{\boldsymbol{\xi}}_n\theta_n}\mathbf{g}_{st_0}$	$\boldsymbol{\xi}_i^{\mathrm{a}} = \mathbf{Ad}_{e^{\widehat{\boldsymbol{\eta}}_i}}\boldsymbol{\xi}_i^{\mathrm{n}};\ \mathbf{g}_{st_0}^{\mathrm{a}} = e^{\widehat{\boldsymbol{\eta}}_{st}}\mathbf{g}_{st_0}^{\mathrm{n}}$	$\left(\delta e^{\widehat{\boldsymbol{\xi}}_i\theta_i} e^{-\widehat{\boldsymbol{\xi}}_i\theta_i}\right)^{\vee} = \left(\mathbf{I} - \mathbf{Ad}_{e^{\widehat{\boldsymbol{\xi}}_i\theta_i}}\right)\delta\boldsymbol{\eta}_i + \boldsymbol{\xi}_i\delta\theta_i$

following additive error update after normalization:

$$\boldsymbol{\xi}^{\mathrm{a}} = \begin{pmatrix} \begin{pmatrix} p_{\mathbf{x}} \\ p_{\mathbf{y}} \\ 0 \end{pmatrix} \times \begin{pmatrix} w_{\mathbf{x}} \\ w_{\mathbf{y}} \\ \sqrt{1 - w_{\mathbf{x}}^2 - w_{\mathbf{y}}^2} \end{pmatrix} \\ \begin{pmatrix} w_{\mathbf{x}} \\ w_{\mathbf{y}} \\ \sqrt{1 - w_{\mathbf{x}}^2 - w_{\mathbf{y}}^2} \end{pmatrix} \end{pmatrix}$$

$$\sim \underbrace{\boldsymbol{e}_6}_{\boldsymbol{\xi}^{\mathrm{n}}} + \underbrace{\frac{1}{\sqrt{1 - w_{\mathbf{x}}^2 - w_{\mathbf{y}}^2}} \begin{pmatrix} (1 - w_{\mathbf{y}}^2)p_{\mathbf{y}} - w_{\mathbf{x}}w_{\mathbf{y}}p_{\mathbf{x}} \\ w_{\mathbf{x}}w_{\mathbf{y}}p_{\mathbf{y}} - (1 - w_{\mathbf{x}}^2)p_{\mathbf{x}} \\ 0 \\ w_{\mathbf{x}} \\ w_{\mathbf{y}} \\ 0 \end{pmatrix}}_{\delta\boldsymbol{\xi}}.$$

The minimal POE approach avoids normalization by a refined error update. In comparison to the Adjoint error model, it parameterizes the ACS manifold only around $\mathbf{e}_6$ (or $\mathbf{e}_3$), and introduces extra local frames during reference frame setup.

4) Local POE Model: Both the local POE approach [see Fig. 12(e)] and the Adjoint error approach adopt the multiplicative error update. In fact, their kinematic and error model can be shown to be equivalent to ours by the following equations ($i = 1, \ldots, n$):

$$\boldsymbol{\xi}_i = \mathbf{Ad}_{\mathbf{h}_i}\mathbf{s}_i,\ \mathbf{g}_{st_0} = \mathbf{h}_{n+1},\ \mathbf{h}_i = \prod_{j=1}^{i} e^{\widehat{\mathbf{p}}_j}$$

$$e^{\delta\widehat{\boldsymbol{\eta}}_i} = \prod_{j=1}^{i}\left(\mathbf{h}_{j-1}e^{\delta\widehat{\mathbf{p}}_j}\mathbf{h}_{j-1}^{-1}\right), e^{\delta\widehat{\boldsymbol{\eta}}_{st}} = \prod_{j=1}^{n+1}\left(e^{\delta\widehat{\mathbf{p}}_j}e^{\widehat{\mathbf{p}}_j}\right). \quad (34)$$

The differentiation of (34) leads to the following equivalence of their calibration Jacobians:

$$\delta\boldsymbol{\eta}_i = \sum_{j=1}^{i}\mathbf{Ad}_{\mathbf{h}_j}\delta\mathbf{p}_j,\ \delta\boldsymbol{\eta}_{st} = \sum_{j=1}^{n+1}\mathbf{Ad}_{\mathbf{h}_j}\delta\mathbf{p}_j.$$

Although being essentially equivalent, the Adjoint error approach stands out with a more geometric formulation, a simpler reference frame setup and the capability to systematically handle both parameter redundancy and additional geometry assumptions on joint axes relations.

5) RLPOE Model: The RLPOE approach shares the same dyad kinematic model with the local POE approach, but implements an additive error model, as in Table I and Fig. 12(f). This explains the difference in their linearization formulas and illustrates the importance of having a suitable error model. In the RLPOE model, Chen *et al.* [20] identified the redundancy of the standard POE model as the projection of elementary errors to the joint twists' column spaces, which is equivalent to (32), the linearization of the Adjoint error model.

VI. SIMULATIONS AND EXPERIMENT

A. Simulation I: 6-DoF Robot Without Noise

In this simulation, we calibrate a Motoman HP20D robot [as in Fig. 13(a)] using the proposed algorithm with pose and point measurements. Parameters of the robot are perturbed from their nominal values to create the actual model, as in Table II. We randomly generate 20 robot configurations and measure the tool frame poses/positions without noise for identification. Another 500 configurations are randomly picked for verification. We plot the mean and maximal error at the verification samples after every iteration in Fig. 14. Our algorithm quickly converges within 3 iterations with very small residuals for both pose and point measurements.

B. Simulation II: 6-DoF Robot With Noises

To validate robustness of our algorithm, we inject Gaussian noise into each calibration measurement with a standard variance of 0.1 mm for the position component and 0.0005 rad for the orientation component. Verification samples are still noise-free. The robot model and sample strategy are the same as in simulation I. Apart from the Adjoint error model, we conduct simulations using the standard POE, minimal POE, local POE, and RLPOE algorithms on the same dataset for comparison, and results are shown in Fig. 15. All algorithms improve the robot's accuracy. The standard POE algorithm produces the largest final mean and maximal errors, and all the other algorithms have similar accuracy performances.

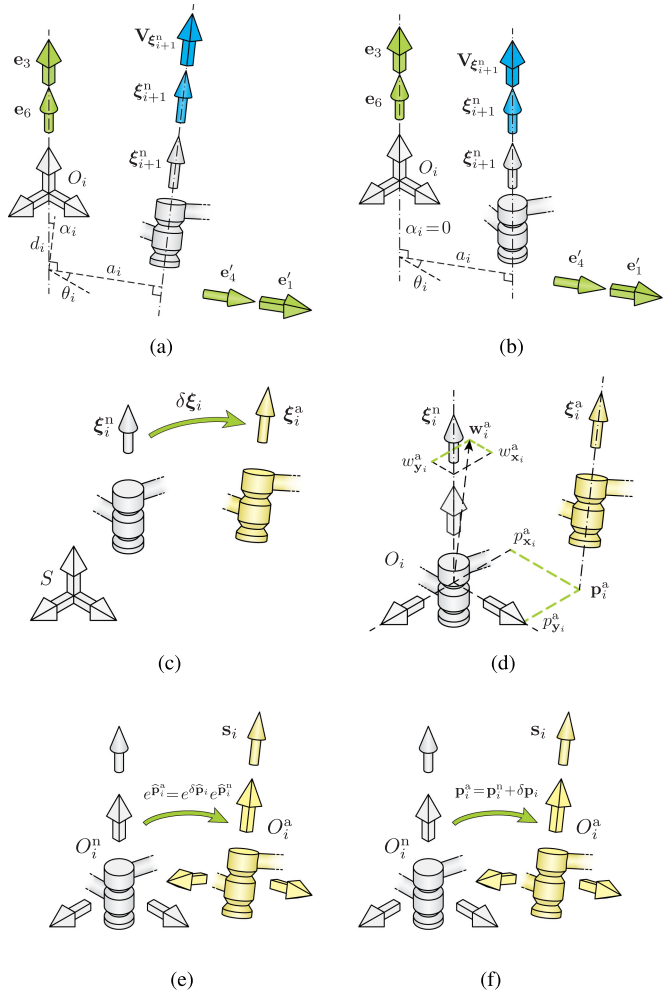

Fig. 12. Errors in the (a) DH model, (b) DH model when consecutive two joints are parallel, (c) standard POE model, (d) minimal POE model, (e) local POE model, and (f) RLPOE model.

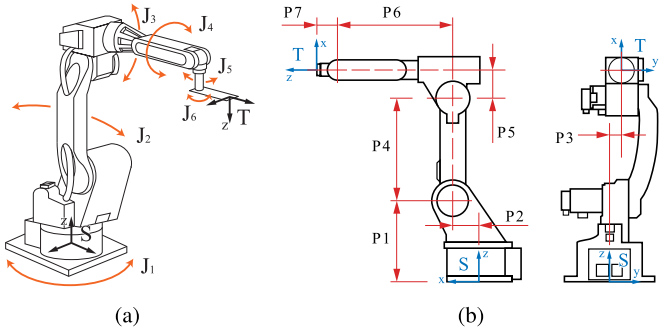

Fig. 13. 6-DoF robot: (a) schematic diagram of Motoman HP20D robot and (b) parameter definition inside Googol GUC controller.

The time elapse for one iteration by each calibration algorithm is shown in Fig. 16. The elapse grows linearly with the number of samples. The Adjoint error and the local POE approach run much faster (with the same precision level) due to elimination of the parameter-varying differentiation. The local POE method runs even a little faster than the Adjoint error approach because no basis matrix needs to be constructed, but at the cost of introducing parameter redundancy.

TABLE II
PARAMETERS OF HP20D ROBOT (UNIT:MM)

J_1	$\boldsymbol{\xi}_1^{\mathrm{n}}$	$(0,0,0,0,0,1)$
	$\boldsymbol{\xi}_1^{\mathrm{a}}$	$(4.986, 2.460, 0.0030, -0.00019, -0.00084, 0.999)$
J_2	$\boldsymbol{\xi}_2^{\mathrm{n}}$	$(-505,0,150,0,1,0)$
	$\boldsymbol{\xi}_2^{\mathrm{a}}$	$(-498.742, -3.964, 153.841, -0.00769, 0.999, 0.00084)$
J_3	$\boldsymbol{\xi}_3^{\mathrm{n}}$	$(-1175,0,150,0,1,0)$
	$\boldsymbol{\xi}_3^{\mathrm{a}}$	$(-1173.08, -9.161, 167.198, -0.00769, 0.999, 0.00084)$
J_4	$\boldsymbol{\xi}_4^{\mathrm{n}}$	$(0,1315,0,1,0,0)$
	$\boldsymbol{\xi}_4^{\mathrm{a}}$	$(-10.1473, 1322.304, 1.694, 0.999, 0.0077, -0.0368)$
J_5	$\boldsymbol{\xi}_5^{\mathrm{n}}$	$(-1315,0,945,0,1,0)$
	$\boldsymbol{\xi}_5^{\mathrm{a}}$	$(-1287.084, -38.923, 958.045, -0.0065, 0.999, 0.0318)$
J_6	$\boldsymbol{\xi}_6^{\mathrm{n}}$	$(0,1315,0,1,0,0)$
	$\boldsymbol{\xi}_6^{\mathrm{a}}$	$(-7.351, 1265.375, -0.135, 0.999, 0.0058, 0.0232)$
T	$\mathbf{g}_{st_0}^{\mathrm{n}}$	$\begin{pmatrix} 0 & -1 & 0 & 1070 \\ 0 & 0 & -1 & 0 \\ 1 & 0 & 0 & 1415 \\ 0 & 0 & 0 & 1 \end{pmatrix}$
	$\mathbf{g}_{st_0}^{\mathrm{a}}$	$\begin{pmatrix} -0.0230 & -0.9997 & 0.0065 & 1087.27 \\ -0.0320 & -0.0058 & -0.9995 & 13.013 \\ 0.9992 & -0.0232 & -0.0318 & 1399.27 \\ 0 & 0 & 0 & 1 \end{pmatrix}$

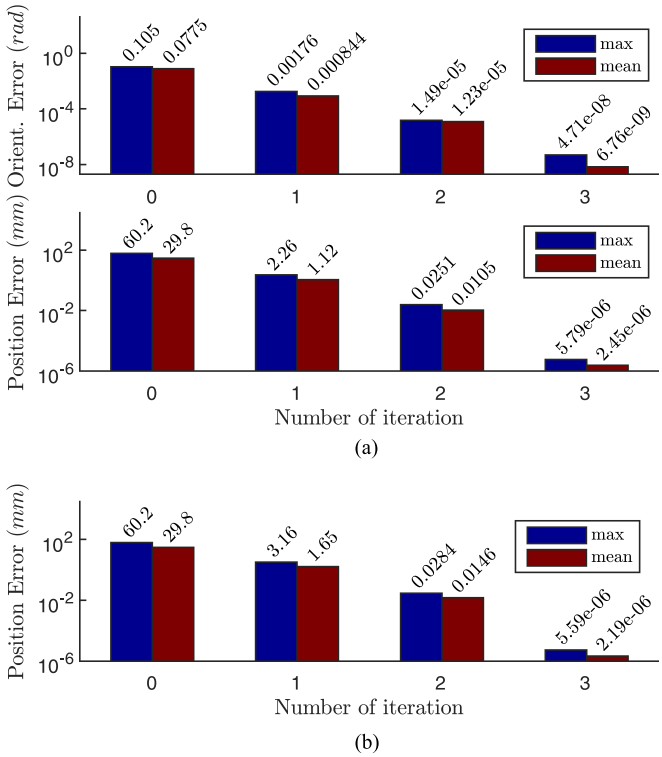

Fig. 14. Verification errors in simulation I with (a) pose measurements and (b) point measurements.

C. Experiment I: SCARA Robot

In this experiment, a Hirata AR-F650H SCARA robot is calibrated with point measurements (as in Fig. 17, with nominal parameters listed in Table III). We use a FARO Laser Tracker ION to acquire the three-dimensional position measurements of an SMR target mounted on the robot end-effector. The resolution and distance measurement accuracy of the laser

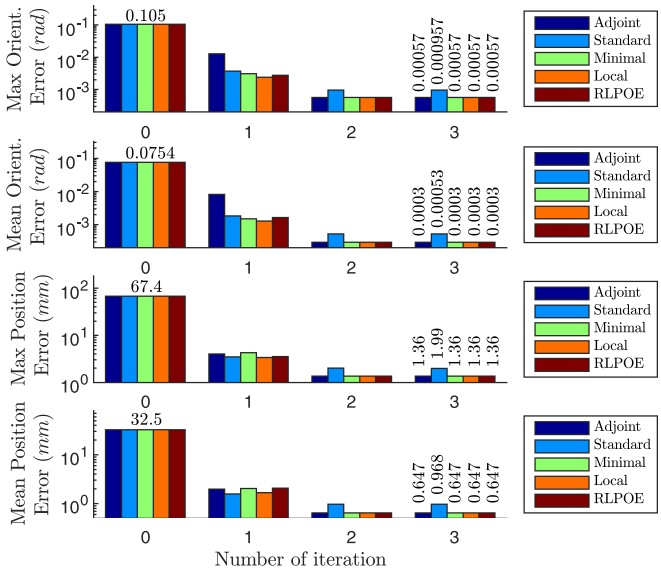

Fig. 15. Verification errors in simulation II.

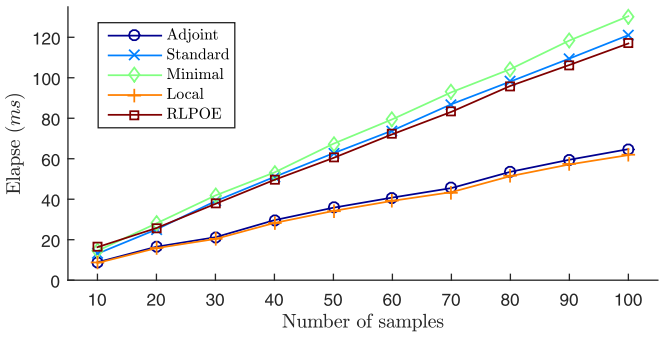

Fig. 16. Average elapse in one iteration in simulation II.

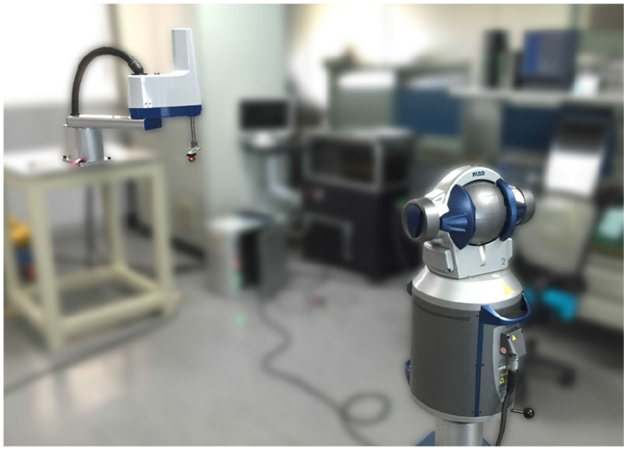

Fig. 17. Setup of the Hirata AR-F650H robot calibration experiment.

tracker are $0.5\,\mu$m and $16\,\mu\text{m} + 0.8\,\mu\text{m/m}$, respectively. The pitch of the robot's last helical joint is assumed to be accurate. Moreover, we assume the last two joints to be parallel, which is implemented in the Adjoint error approach and ignored in other algorithms. 100 samples are taken within the robot workspace,

TABLE III
NOMINAL PARAMETERS OF HIRATA AR-F650H ROBOT (UNIT:MM)

J_1	$\boldsymbol{\xi}_1^{\text{n}}$	$(0, 0, 0, 0, 0, 1)$
J_2	$\boldsymbol{\xi}_2^{\text{n}}$	$(400, 0, 0, 0, 0, 1)$
J_3	$\boldsymbol{\xi}_3^{\text{n}}$	$(0, 0, -1, 0, 0, 0)$
J_4	$\boldsymbol{\xi}_4^{\text{n}}$	$(-650, 0, -3.183, 0, 0, -1)$
T	$\mathbf{q}_{e_0}^{\text{n}}$	$(0, 750, 170)$

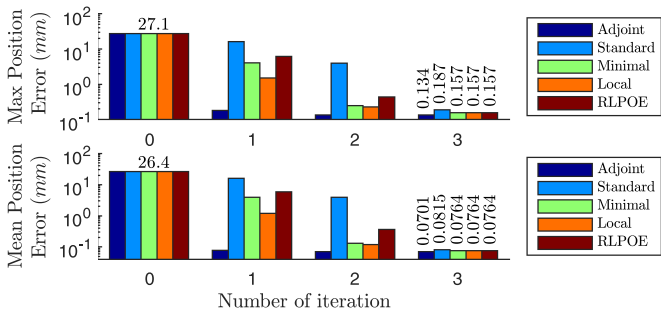

Fig. 18. Verification errors in experiment I.

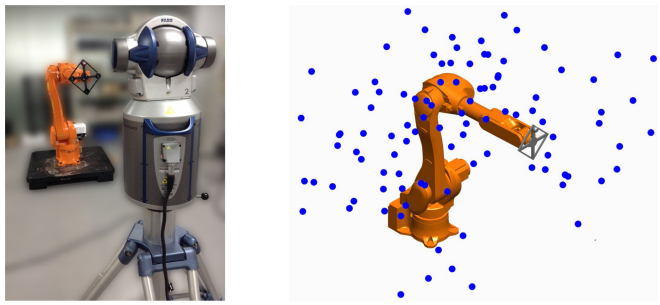

(a) (b)

Fig. 19. Calibration experiment on a 6-DoF robot: (a) setup of the Kawasaki RA10N robot and FARO laser tracker ION; (b) sample set.

of which 50 samples are used to identify the robot parameters and the rest for verification.

As shown in Fig. 18, all calibration algorithms converge successfully; the Adjoint error approach results in better accuracy restoration than the others since it takes advantage of the geometric relation between joints. This illustrates the benefit of having reliable prior information. The final accuracy with a mean value 0.07 mm is adequate for 3C manufacturing tasks such as labeling and snap-fitting.

D. Experiment II: 6-DoF Robot

We calibrate a Kawasaki RA10N robot with 100 point measurements as in Fig. 19. A Googol GUC controller with a built-in 6-DoF robot model [see Fig. 13(b)] is used to control the robot. From the parameter definition, the following prior information is assumed implicitly at initial configuration.

1) The axes of joint 1 and 2 are perpendicular.
2) The axes of joint 2 and 3 are parallel.
3) The axes of joint 3 and 4 are perpendicular.

TABLE IV
NOMINAL PARAMETERS OF RA10N ROBOT (UNIT:MM)

P1	P2	P3	P4	P5	P6	P7	$q_{e_{\mathbf{x}0}}$	$q_{e_{\mathbf{y}0}}$	$q_{e_{\mathbf{z}0}}$
430	100	0	650	0	700	88	928	0	1200

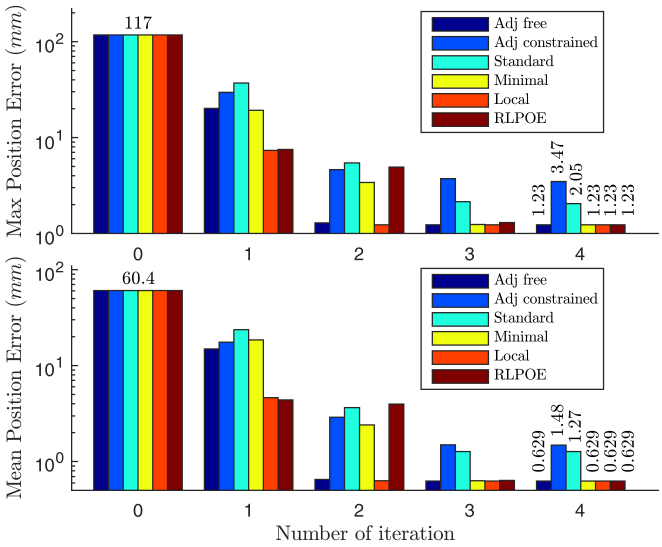

Fig. 20. Verification errors in experiment II.

4) The axes of joint 4 and 5 are perpendicular.
5) The axes of joint 5 and 6 are perpendicular.
6) The axes of joint 4, 5, and 6 intersect at one point.

The nominal parameters and the initial position of the measurement point in the base frame are listed in Table IV.

Of all the 100 samples, 50 are used for calibration and the rest for verification. We run the Adjoint error calibration algorithm both with and without the joint relation assumptions, which we refer to as *Adjoint free* and *Adjoint constrained*, respectively. Since all the joints are under parallel or perpendicular restrictions, a rotational basis $\mathbf{B}_r = (\mathbf{e}_4, \mathbf{e}_5, \mathbf{e}_6)$ is assigned to the whole robot. Bases $\boldsymbol{\xi}_3^{\mathrm{n}}$, $\boldsymbol{\xi}_4^{\mathrm{n}}$, and $\boldsymbol{\xi}_5^{\mathrm{n}}$ are introduced in particular to handle the perpendicular assumptions. The last three joints vary together with their intersection point and thus have the same translational basis $\mathbf{B}_t = (\mathbf{e}_1, \mathbf{e}_2, \mathbf{e}_3)$. Therefore, the basis matrix is given by

$$\mathbf{B} = \begin{pmatrix} \mathbf{B}_r & \mathbf{B}_{1,t} & \mathbf{0} & \mathbf{0} & 0 & 0 & 0 & 0 & 0 \\ \mathbf{B}_r & \mathbf{0} & \mathbf{B}_{2,t} & \mathbf{0} & 0 & 0 & 0 & 0 & 0 \\ \mathbf{B}_r & \mathbf{0} & \mathbf{0} & \mathbf{B}_{3,t} & 0 & 0 & 0 & 0 & 0 \\ \mathbf{B}_r & \mathbf{0} & \mathbf{0} & \mathbf{0} & \boldsymbol{\xi}_3^{\mathrm{n}} & 0 & 0 & \mathbf{B}_t & 0 \\ \mathbf{B}_r & \mathbf{0} & \mathbf{0} & \mathbf{0} & 0 & \boldsymbol{\xi}_4^{\mathrm{n}} & 0 & \mathbf{B}_t & 0 \\ \mathbf{B}_r & \mathbf{0} & \mathbf{0} & \mathbf{0} & 0 & 0 & \boldsymbol{\xi}_5^{\mathrm{n}} & \mathbf{B}_t & 0 \\ \mathbf{0} & \mathbf{0} & \mathbf{0} & \mathbf{0} & 0 & 0 & 0 & 0 & \mathbf{E}_{st} \end{pmatrix}_{39\times 18}.$$

The verification errors after each iteration are shown in Fig. 20. The initial error is quite large since it includes not only the robot accuracy error but also the estimation error of the transformation between the robot base frame and laser tracker frame. After calibration, the mean of the total positioning error is about 0.63 mm by the minimal POE, local POE, and RLPOE methods, and the Adjoint free approach. If the joint relation assumptions are imposed, the performance is comparatively worse: the mean positioning error is about 1.5 mm. This implies that actual joint relations do not satisfy the assumptions used in the robot controller. The robot's absolute accuracy with joint relation constraints is not good for 3C tasks with a very high precision requirement such as dispensing. Nevertheless, if such a calibration performance is acceptable, for instance, for screw-driving operations, we can directly modify the controller parameters under its restriction and no external PC is needed.

TABLE V
COMPARISON OF DIFFERENT POE-BASED CALIBRATION METHODS

	Standard POE	Minimal POE	Local POE	RLPOE	Adjoint Error
Convergence	✓	✓	✓	✓	✓
High Accuracy		✓	✓	✓	✓
High Efficiency			✓		✓
Simple Frame Setup	✓				✓
Easy Constraints Handling					✓
Agreement with ACS					✓

VII. CONCLUSION

In this paper, we propose a novel POE-based robot kinematic calibration algorithm based on the ACS model and Adjoint error update. We give an explicit characterization of the ACS manifolds, and introduce the multiplicative Adjoint error for joint twists. The Adjoint error model automatically eliminates parameter redundancy of joint twist coordinates and the computationally intensive parameter-varying differentiation operations. We give a rigorous proof of the parameter identifiability of the proposed algorithm with both pose and point measurements. Additional geometric assumptions on joint axes relations can also be easily handled by modifying the basis matrix promptly.

We also use the same geometric framework for a comparative study of existing kinematic calibration algorithms. As in Table V, the proposed algorithm stands out in terms of efficiency by avoiding parameter-varying differentiations; ease of implementation with only one reference frame and one tool frame in comparison to multiple local link frames in the other methods; capability to handle geometric constraints on joint axes relations; conformation to the nonlinear geometry of the ACS manifold, based on which our algorithm is developed. Simulations and experiments are presented to support our claims.

APPENDIX A
LIE GROUP STRUCTURE OF $\mathbf{T}(\mathbf{SO}(\mathbf{3}))$ AND THE TRANSITIVE ACTION $\Psi_{\mathcal{R}}$

A. $\mathbf{T}(\mathbf{SO}(\mathbf{3}))$ *is a Lie Group*

The group operation of $\mathbf{T}(\mathbf{SO}(\mathbf{3}))$ is given by

$$\star : \mathbf{T}(\mathbf{SO}(\mathbf{3})) \times \mathbf{T}(\mathbf{SO}(\mathbf{3})) \to \mathbf{T}(\mathbf{SO}(\mathbf{3}))$$
$$((\mathbf{R}_1, \mathbf{V}_{\mathbf{R}_1}), (\mathbf{R}_2, \mathbf{V}_{\mathbf{R}_2})) \mapsto (\mathbf{R}_1\mathbf{R}_2, \underbrace{\mathbf{V}_{\mathbf{R}_1}\mathbf{R}_2 + \mathbf{R}_1\mathbf{V}_{\mathbf{R}_2}}_{\text{Leibniz's product rule}}).$$

For any two elements $(\mathbf{R}_1, \mathbf{V}_{\mathbf{R}_1}), (\mathbf{R}_2, \mathbf{V}_{\mathbf{R}_2}) \in \mathbf{T}(\mathbf{SO(3)})$,

$$(\mathbf{R}_1, \mathbf{V}_{\mathbf{R}_1}) \star (\mathbf{R}_2, \mathbf{V}_{\mathbf{R}_2}) \triangleq (\mathbf{R}_1\mathbf{R}_2, \mathbf{V}_{\mathbf{R}_1}\mathbf{R}_2 + \mathbf{R}_1\mathbf{V}_{\mathbf{R}_2})$$

indeed defines another element in $\mathbf{T}(\mathbf{SO(3)})$, since

$$\begin{aligned}(\mathbf{V}_{\mathbf{R}_1}\mathbf{R}_2 + \mathbf{R}_1\mathbf{V}_{\mathbf{R}_2})(\mathbf{R}_1\mathbf{R}_2)^{\mathrm{T}} \\ = \mathbf{V}_{\mathbf{R}_1}\mathbf{R}_1^{\mathrm{T}} + \mathbf{R}_1(\mathbf{V}_{\mathbf{R}_2}\mathbf{R}_2^{\mathrm{T}})\mathbf{R}_1^{\mathrm{T}} \in \mathbf{so(3)}.\end{aligned}$$

It is easy to verify that the identity element and inverse of $(\mathbf{R}, \mathbf{V}_{\mathbf{R}})$ are given by $(\mathbf{I}_{3\times3}, \mathbf{0}_{3\times3})$ and $(\mathbf{R}^{\mathrm{T}}, -\mathbf{R}^{\mathrm{T}}\mathbf{V}_{\mathbf{R}}\mathbf{R}^{\mathrm{T}})$, respectively. The Lie group structure is exactly the same as that of the semi-direct product $\mathbf{SO(3)} \ltimes \mathbf{so(3)} \simeq \mathbf{SO(3)} \ltimes \mathbb{R}^3$ with respect to Adjoint action [26, Definition 9.2.22]. In other words, $\mathbf{T}(\mathbf{SO(3)})$ is isomorphic to $\mathbf{SE(3)}$.

B. $\Psi_{\mathcal{R}}$ as in (5) is a Transitive Action

It is easy to verify that $\Psi_{\mathcal{R}}$ defines a Lie group action by Leibnitz's product rule. To see it is transitive we only need to verify that $\forall (\mathbf{w}_1, \mathbf{v}_{\mathbf{w}_1}), (\mathbf{w}_2, \mathbf{v}_{\mathbf{w}_2}) \in \mathbf{T}(\mathbf{S}^2), \exists (\mathbf{R}, \mathbf{V}_{\mathbf{R}})$, such that $\mathbf{w}_2 = \mathbf{R}\mathbf{w}_1$ (by transitivity of $\Psi_{\mathcal{P}}$) and

$$\mathbf{v}_{\mathbf{w}_2} = \mathbf{V}_{\mathbf{R}}\mathbf{w}_1 + \mathbf{R}\mathbf{v}_{\mathbf{w}_1}.$$

Since $\mathbf{V}_{\mathbf{R}} = \widehat{\mathbf{p}}\mathbf{R}$ for some $\mathbf{p} \in \mathbb{R}^3$ as in (6), we have

$$\mathbf{v}_{\mathbf{w}_2} = \mathbf{V}_{\mathbf{R}}\mathbf{w}_1 + \mathbf{R}\mathbf{v}_{\mathbf{w}_1} = \widehat{\mathbf{p}}\mathbf{R}\mathbf{w}_1 + \mathbf{R}\mathbf{v}_{\mathbf{w}_1} = \widehat{\mathbf{p}}\mathbf{w}_2 + \mathbf{R}\mathbf{v}_{\mathbf{w}_1}.$$

A solution of $\mathbf{p}$ (not unique) is given by

$$\mathbf{p} = \mathbf{w_2} \times (\mathbf{v}_{\mathbf{w_2}} - \mathbf{R}\mathbf{v}_{\mathbf{w_1}}).$$

Appendix B
Identifiability With Pose Measurements

We first prove the following lemma.

Lemma 1: When $\theta \neq 2\pi\mathbb{Z}$

$$\mathrm{Im}(\mathbf{B}) \cap \ker(\mathbf{I} - \mathbf{Ad}_{e^{\widehat{\boldsymbol{\xi}}\theta}}) = \{\mathbf{0}\}.$$

Proof: When $\theta \neq 2\pi\mathbb{Z}$, $\mathbf{Ad}_{e^{\widehat{\boldsymbol{\xi}}\theta}} \neq \mathbf{I}$ which avoids the trivial case. For a prismatic joint $\boldsymbol{\xi}$, it is by straightforward computation to see that $\ker(\mathbf{I} - \mathbf{Ad}_{e^{\widehat{\boldsymbol{\xi}}\theta}}) = \mathfrak{x}(\boldsymbol{\xi})$. Similarly, $\ker(\mathbf{I} - \mathbf{Ad}_{e^{\widehat{\boldsymbol{\xi}}\theta}}) = \mathfrak{c}(\boldsymbol{\xi})$ for a revolute or helical joint $\boldsymbol{\xi}$. The lemma is then proved since the span of columns of our basis matrix $\mathbf{B}$ is complementary to $\mathfrak{c}(\boldsymbol{\xi})$ (or $\mathfrak{x}(\boldsymbol{\xi})$). ■

Let us take $r + t + 1 = n + 1$ samples as

$$\begin{cases} \boldsymbol{\Theta}^i = \begin{pmatrix} 0 & \cdots & 0 & \theta_i & 0 & \cdots & 0 \end{pmatrix}^{\mathrm{T}} \\ \qquad i = 1, \ldots, n,\ \theta_i \neq 2\pi\mathbb{Z} \\ \boldsymbol{\Theta}^{n+1} = \begin{pmatrix} 0 & \cdots & 0 \end{pmatrix}^{\mathrm{T}} \end{cases}$$

where the superscript $1, \ldots, n+1$ indicates sample numbering. We will prove that the calibration Jacobian matrix $\mathbb{A}$ is of full column rank by contradiction.

If $\mathbb{A}$ is not of full column rank, we can find a nonzero vector $\mathbf{k} = (\mathbf{k}_1^{\mathrm{T}}, \cdots, \mathbf{k}_n^{\mathrm{T}}, \mathbf{k}_{st}^{\mathrm{T}})^{\mathrm{T}}$, such that $\mathbb{A}\mathbf{k} = \mathbf{0}$. In each sample

$$\begin{cases} \mathbf{A^{n+1}k} = \mathbf{k_{st}} = \mathbf{0} \\ \mathbf{A}^i\mathbf{k} = (\mathbf{I} - \mathbf{Ad}_{e^{\widehat{\boldsymbol{\xi}}_i \boldsymbol{\theta}_i}})\mathbf{B}_i\mathbf{k}_i = \mathbf{0},\ i = 1, \ldots, n. \end{cases}$$

By Lemma 1, $\mathbf{k}_i = \mathbf{0}, i = 1, \ldots, n$ and therefore $\mathbf{k} = \mathbf{0}$, which is a contradiction. Therefore, all the $4r + 2t + 6$ parameters in $\mathbf{k}$ are identifiable with these $r + t + 1$ samples.

Appendix C
Identifiability With Point Measurements

A. Initial Tool Frame Orientation Cannot be Recovered

Define $\mathbf{Q}_{st}$ by

$$\mathbf{Q}_{st} = \mathbf{Ad}_n = \begin{pmatrix} \mathbf{R_n} & \widehat{\mathbf{p}}_n\mathbf{R}_n \\ \mathbf{0} & \mathbf{R}_n \end{pmatrix}.$$

Since $\mathbf{q}_e^{\mathrm{n}} = \mathbf{R}_n\mathbf{q}_{e_0}^{\mathrm{n}} + \mathbf{p}_n$, we have

$$\left(\mathbf{I} - \widehat{\mathbf{q}}_{\mathbf{e}}^{\mathrm{n}}\right)\mathbf{Q}_{st} = \begin{pmatrix} \mathbf{R}_n & -\mathbf{R}_n\widehat{\mathbf{q}}_{e_0}^{\mathrm{n}} \end{pmatrix}$$

where the constant $\mathbf{q}_{e_0}^{\mathrm{n}}$ is the initial tool frame position as in (27). Since the last three columns always depend linearly on the first three, the initial tool frame orientation cannot be recovered.

B. Identifiability of $\mathbf{k}$ in (26)

We first prove the following lemma.

Lemma 2: Given a prismatic joint $\boldsymbol{\xi}$

$$\ker\left(\begin{pmatrix} \mathbf{I} & -\widehat{\mathbf{q}}_e \end{pmatrix}\left(\mathbf{I} - \mathbf{Ad}_{e^{\widehat{\boldsymbol{\xi}}\theta}}\right)\right) = \mathfrak{x}(\boldsymbol{\xi}), \quad \theta \neq 0.$$

For a revolute or helical joint $\boldsymbol{\xi}$, if $\theta \neq 2\pi\mathbb{Z}$ and the initial point position $\mathbf{q}_{e_0}$ does not lie on $\boldsymbol{\xi}$, then

$$\ker\left(\begin{pmatrix} \mathbf{I} & -\widehat{\mathbf{q}}_e \end{pmatrix}(\mathbf{I} - \mathbf{Ad}_{e^{\hat{\xi}\theta}})\right) = \mathfrak{c}(\boldsymbol{\xi}) \oplus \left\{\begin{pmatrix} \boldsymbol{\nu} \\ \boldsymbol{\mu} \end{pmatrix}\right\}_{\mathrm{sp}}$$

where

$$\begin{aligned} \boldsymbol{\mu} &= e^{\widehat{\mathbf{w}}(\pi-\theta)/2}(\mathbf{I} - \mathbf{w}\mathbf{w}^{\mathrm{T}})(\mathbf{q}_e - \mathbf{q}) \\ \boldsymbol{\nu} &= \frac{e^{\widehat{\mathbf{w}}(\pi-\theta)/2}}{2\sin(\theta/2)}(\widehat{\mathbf{p}}\mathbf{R} + \widehat{\mathbf{q}}_e(\mathbf{I} - \mathbf{R}))\,\boldsymbol{\mu} \\ \boldsymbol{\xi} &= \begin{pmatrix} \mathbf{v} \\ \mathbf{w} \end{pmatrix},\ \mathbf{q} = \mathbf{w}\times\mathbf{v},\ e^{\widehat{\boldsymbol{\xi}}\theta} = \begin{pmatrix} \mathbf{R} & \mathbf{p} \\ \mathbf{0}_{1\times3} & 1 \end{pmatrix} \\ \mathbf{R} &= e^{\widehat{\mathbf{w}}\theta},\ \mathbf{p} = (\mathbf{I} - \mathbf{R})\mathbf{q} + (\mathbf{w}^{\mathrm{T}}\mathbf{v}\theta)\mathbf{w}. \end{aligned}$$

If $\mathbf{q}_{e_0}$ lies on $\boldsymbol{\xi}$,

$$\ker\left((\mathbf{I} - \widehat{\mathbf{q}}_e)(\mathbf{I} - \mathbf{Ad}_{e^{\widehat{\boldsymbol{\xi}}\theta}})\right) = \mathfrak{c}(\boldsymbol{\xi}) \oplus \left\{\begin{pmatrix} \boldsymbol{\kappa}_1 \\ \mathbf{w}_1 \end{pmatrix}, \begin{pmatrix} \boldsymbol{\kappa}_2 \\ \mathbf{w}_2 \end{pmatrix}\right\}_{\mathrm{sp}}$$

where

$$\boldsymbol{\kappa}_i = (\mathbf{I} - \mathbf{w}\mathbf{w}^{\mathrm{T}})\widehat{\mathbf{q}}_{e_0}\mathbf{w}_i + \frac{e^{\widehat{\mathbf{w}}(\pi-\theta)/2}}{2\sin(\theta/2)}(\mathbf{w}^{\mathrm{T}}\mathbf{v}\theta)\widehat{\mathbf{w}}\mathbf{w}_i, i = 1, 2$$

and $\mathbf{w}$, $\mathbf{w}_1$, and $\mathbf{w}_2$ are mutually orthogonal. ♢

Proof: For a prismatic joint $\boldsymbol{\xi}$

$$\begin{pmatrix} \mathbf{I} & -\widehat{\mathbf{q}}_e \end{pmatrix}(\mathbf{I} - \mathbf{Ad}_{e^{\hat{\xi}\theta}}) = \begin{pmatrix} \mathbf{0} & -\widehat{\mathbf{v}}\theta \end{pmatrix},\ \boldsymbol{\xi} = \begin{pmatrix} \mathbf{v} \\ \mathbf{0} \end{pmatrix},\ \theta \neq 0$$

and therefore

$$\ker\left(\begin{pmatrix} \mathbf{I} & -\widehat{\mathbf{q}}_e \end{pmatrix}(\mathbf{I} - \mathbf{Ad}_{e^{\hat{\xi}\theta}})\right) = \mathfrak{x}(\boldsymbol{\xi}).$$

For a revolute or helical joint $\boldsymbol{\xi}$, we consider only the nontrivial case $\theta \neq 2\pi\mathbb{Z}$. It is clear that

$$\ker\left(\begin{pmatrix}\mathbf{I} & -\widehat{\mathbf{q}}_e\end{pmatrix}(\mathbf{I}-\mathbf{Ad}_{e^{\hat{\boldsymbol{\xi}}\theta}})\right) \supset \ker\left(\mathbf{I}-\mathbf{Ad}_{e^{\hat{\boldsymbol{\xi}}\theta}}\right) = \mathfrak{c}(\boldsymbol{\xi})$$

and we will find the remaining null subspaces by solving

$$\begin{pmatrix}\mathbf{I} & -\widehat{\mathbf{q}}_e\end{pmatrix}(\mathbf{I}-\mathbf{Ad}_{e^{\hat{\boldsymbol{\xi}}\theta}})\boldsymbol{\zeta} = \mathbf{0}$$

$$\boldsymbol{\xi} = \begin{pmatrix}\mathbf{v}\\ \mathbf{w}\end{pmatrix}, \boldsymbol{\zeta} = \begin{pmatrix}\mathbf{u}_1\\ \mathbf{u}_2\end{pmatrix}, \mathbf{u}_1 \perp \mathbf{w}, \mathbf{u}_2 \perp \mathbf{w}.$$

This equation can be rewritten as

$$\begin{aligned}(\mathbf{I}-\mathbf{R})\mathbf{u}_1 &= (\widehat{\mathbf{p}}\mathbf{R} + \widehat{\mathbf{q}}_e(\mathbf{I}-\mathbf{R}))\,\mathbf{u}_2\\ &= \left((\widehat{\mathbf{q}}_e-\widehat{\mathbf{q}})(\mathbf{I}-\mathbf{R}) + (\mathbf{I}-\mathbf{R})\widehat{\mathbf{q}} + (\mathbf{w}^{\mathrm{T}}\mathbf{v}\theta)\widehat{\mathbf{w}}\mathbf{R}\right)\mathbf{u}_2 \quad (35)\end{aligned}$$

where $\mathbf{q}$ is a point on the joint axis. Since

$$(\mathbf{I}-\mathbf{R})\mathbf{x} = 2\sin(\theta/2)e^{\widehat{\mathbf{w}}(\theta-\pi)/2}(\mathbf{I}-\mathbf{w}\mathbf{w}^{\mathrm{T}})\mathbf{x}$$

$\forall \mathbf{x} \in \mathbb{R}^3$, we see that both $(\mathbf{I}-\mathbf{R})\mathbf{u}_1$ and $((\mathbf{I}-\mathbf{R})\widehat{\mathbf{q}} + (\mathbf{w}^{\mathrm{T}}\mathbf{v}\theta)\widehat{\mathbf{w}}\mathbf{R})\mathbf{u}_2$ are orthogonal to $\mathbf{w}$. If $\mathbf{q}_{e_0}$ does not lie on the axis of $\boldsymbol{\xi}$, (35) holds only when $\mathbf{w}^{\mathrm{T}}(\widehat{\mathbf{q}}_e-\widehat{\mathbf{q}})(\mathbf{I}-\mathbf{R})\mathbf{u}_2 = 0$, which leads to $\mathbf{u}_2 = \boldsymbol{\mu}$ and $\mathbf{u}_1 = \boldsymbol{\nu}$. If, on the other hand, $\mathbf{q}_{e_0}$ lies on the axis of $\boldsymbol{\xi}$, with $\mathbf{R}\widehat{\mathbf{w}}\mathbf{R}^{\mathrm{T}} = (\mathbf{R}\mathbf{w})^{\wedge} = \widehat{\mathbf{w}}$ [8] and $\mathbf{q}_e = \mathbf{q}_{e_0} + (\mathbf{w}^{\mathrm{T}}\mathbf{v}\theta)\mathbf{w}$, (35) can be simplified into

$$(\mathbf{I}-\mathbf{R})\mathbf{u}_1 = \left((\mathbf{I}-\mathbf{R})\widehat{\mathbf{q}}_{e_0} + (\mathbf{w}^{\mathrm{T}}\mathbf{v}\theta)\widehat{\mathbf{w}}\right)\mathbf{u}_2.$$

Then we have $\mathbf{u}_2 \in \{\mathbf{w}_1, \mathbf{w}_2\}_{\mathrm{sp}}$ and $\mathbf{u}_1 = \boldsymbol{\kappa}_i$. ■

Now we proceed with the proof of Theorem 2 by contradiction using the induction method (with $2r+t+1$ samples). If $\mathbb{A}$ is not full column rank, we can find a nonzero vector $\mathbf{k} = (\mathbf{k}_1^{\mathrm{T}}, \cdots, \mathbf{k}_n^{\mathrm{T}}, \mathbf{k}_{st}^{\mathrm{T}})^{\mathrm{T}}$ such that $\mathbb{A}\mathbf{k} = \mathbf{0}$.

1) We take $\boldsymbol{\Theta}^{2r+t+1} = (0, \cdots, 0)^{\mathrm{T}}$, then $\mathbf{k}_{st} = \mathbf{0}$.
2) For $\mathbf{k}_n$, we may have the following cases:
   a) $\boldsymbol{\xi}_n$ is a prismatic joint. Take $\boldsymbol{\Theta}^t = (0, \cdots, 0, \theta_n)^{\mathrm{T}}$, $\theta_n \neq 0$ and we have $\mathbf{k}_n = \mathbf{0}$ following Appendix B.
   b) $\boldsymbol{\xi}_n$ is a revolute or helical joint, and the measurement point does not lie on its axis. We take

$$\begin{aligned}\boldsymbol{\Theta}^{2r+t-1} &= (0, \cdots, 0, \theta_n^1)^{\mathrm{T}}\\ \boldsymbol{\Theta}^{2r+t} &= (0, \cdots, 0, \theta_n^2)^{\mathrm{T}}\\ \theta_n^1 \neq 2\pi\mathbb{Z},\ \theta_n^2 &\neq 2\pi\mathbb{Z}, \theta_n^1 - \theta_n^2 \neq 2\pi\mathbb{Z}. \quad (36)\end{aligned}$$

   Note that $\boldsymbol{\mu}$ in Lemma 2 rotates at an angle of $\theta/2$, so the intersection of null spaces leaves only $\mathfrak{c}(\boldsymbol{\xi}_n)$. With the basis matrix $\mathbf{B}_n$, $\mathbf{k}_n = \mathbf{0}$.
   c) $\boldsymbol{\xi}_n$ is a helical joint with nonzero pitch, and the measurement point lies on its axis. We take two samples as in (36), and we can always find θ_n^1, θ_n^2, such that $\boldsymbol{\kappa}_i^1 \neq \boldsymbol{\kappa}_i^2$ with difference $(\boldsymbol{\kappa}_i^1 - \boldsymbol{\kappa}_i^2) \perp \mathbf{w}$. Therefore, the common null space of these two samples is $\mathfrak{c}(\boldsymbol{\xi})$, and $\mathbf{k}_n = \mathbf{0}$ due to the basis matrix $\mathbf{B}_n$.

As a corollary, if $\mathbf{q}_{e_0}$ lies on the axis of the last revolute joint, there would be an extra 2-D subspace in the null space. That is because $\boldsymbol{\kappa}_i$ does not vary with joint angle θ_n when the pitch is zero.

3) Assume that $\mathbf{k}_j = \mathbf{0}, j = i+1, \ldots, n$, then for $\mathbf{k}_i$, we may have the following cases:

   a) $\boldsymbol{\xi}_i$ is the $\mathcal{P}_i$th prismatic joint. We can take $\boldsymbol{\Theta}^{\mathcal{P}_i} = (0, \cdots, 0, \theta_i, 0, \cdots, 0)^{\mathrm{T}}$ and then $\mathbf{k}_i = \mathbf{0}$ by Appendix B.
   b) $\boldsymbol{\xi}_i$ is the $\mathcal{R}_i$th revolute or helical joint, and the measurement point can be moved away from its axis by some later joints $\boldsymbol{\xi}_j, j > i$. We take two samples:

$$\begin{aligned}\boldsymbol{\Theta}^{2\mathcal{R}_i+t-1} &= (0, \cdots, 0, \theta_i^1, *)^{\mathrm{T}}\\ \boldsymbol{\Theta}^{2\mathcal{R}_i+t} &= (0, \cdots, 0, \theta_i^2, *)^{\mathrm{T}}\\ \theta_i^1 \neq 2\pi\mathbb{Z},\ \theta_i^2 &\neq 2\pi\mathbb{Z},\ \theta_i^1 - \theta_i^2 \neq 2\pi\mathbb{Z}. \quad (37)\end{aligned}$$

      We use the joint angles in $*$ to move the measurement point away from the axis of joint $\boldsymbol{\xi}_i$. Because $\mathbf{k}_j = \mathbf{0}, j > i$, we can prove $\mathbf{k}_i = \mathbf{0}$ by following (2.2).
   c) $\boldsymbol{\xi}_i$ is the $\mathcal{R}_i$th revolute or helical joint, and the measurement point cannot be moved away from its axis. In this case, we can only move the measurement point along the axis by $\boldsymbol{\xi}_j, j > i$. We take samples as in (37), and use $\boldsymbol{\xi}_j$ to behave as the "joint pitch." As $\mathbf{k}_j = \mathbf{0}, j > i$, we can get $\mathbf{k}_i = \mathbf{0}$ by following (2.c).

By mathematical induction, $\mathbf{k}_i = \mathbf{0}, i = 1, \ldots, n$ and therefore $\mathbf{k} = \mathbf{0}$, which contradicts our assumption. As a result, all the $4r+2t+3$ parameters in $\mathbf{k}$ are identifiable under the condition of Theorem 2 with these $2r+t+1$ samples.

Appendix D
$\delta\boldsymbol{\xi} \in \mathfrak{c}(\boldsymbol{\xi}^{\mathrm{n}})$ Takes No Effect After an Additive Error Update

After an additive error update

$$\boldsymbol{\xi}^{\mathrm{a}} = \begin{pmatrix}\mathbf{v}^{\mathrm{a}}\\ \mathbf{w}^{\mathrm{a}}\end{pmatrix} \sim \boldsymbol{\xi}^{\mathrm{n}} + \delta\boldsymbol{\xi} = \begin{pmatrix}\mathbf{v}^{\mathrm{n}} + a_1\mathbf{v}^{\mathrm{n}} + a_2\mathbf{w}^{\mathrm{n}}\\ \mathbf{w}^{\mathrm{n}} + a_1\mathbf{w}^{\mathrm{n}}\end{pmatrix}$$

$$\boldsymbol{\xi}^{\mathrm{n}} = \begin{pmatrix}\mathbf{v}^{\mathrm{n}}\\ \mathbf{w}^{\mathrm{n}}\end{pmatrix},\ \delta\boldsymbol{\xi} = a_1\begin{pmatrix}\mathbf{v}^{\mathrm{n}}\\ \mathbf{w}^{\mathrm{n}}\end{pmatrix} + a_2\begin{pmatrix}\mathbf{w}^{\mathrm{n}}\\ \mathbf{0}\end{pmatrix} \in \mathfrak{c}(\boldsymbol{\xi}^{\mathrm{n}}).$$

Impose constraint (2) and we have $\mathbf{w}^{\mathrm{a}} = \mathbf{w}^{\mathrm{n}}$. Impose constraint (3) and we obtain

$$\mathbf{v}^{\mathrm{a}} = \left(\mathbf{I} - \mathbf{w}^{\mathrm{n}}(\mathbf{w}^{\mathrm{n}})^{\mathrm{T}}\right)\left(\mathbf{v}^{\mathrm{n}} + \frac{a_2}{1+a_1}\mathbf{w}^{\mathrm{n}}\right).$$

Since $\mathbf{v}^{\mathrm{n}} \perp \mathbf{w}^{\mathrm{n}}$, $\mathbf{v}^{\mathrm{a}} = \mathbf{v}^{\mathrm{n}}$. Therefore, $\boldsymbol{\xi}^{\mathrm{a}} = \boldsymbol{\xi}^{\mathrm{n}}$ after the normalization process.

References

[1] B. Karan and M. Vukobratović, "Calibration and accuracy of manipulation robot models—An overview," *Mechanism Mach. Theory*, vol. 29, no. 3, pp. 479–500, 1994.
[2] B. W. Mooring, Z. S. Roth, and M. R. Driels, *Fundamentals of Manipulator Calibration*. Hoboken, NJ, USA: Wiley, 1991.
[3] Z. S. Roth, B. Mooring, and B. Ravani, "An overview of robot calibration," *IEEE J. Robot. Autom.*, vol. 3, no. 5, pp. 377–385, Oct. 1987.
[4] R. P. Paul, *Robot Manipulators: Mathematics, Programming, and Control*. Cambridge, MA, USA: MIT Press, 1981.
[5] S. Hayati, "Robot arm geometric link parameter estimation," in *Proc. IEEE Decision Control*, 1983, vol. 22, pp. 1477–1483.
[6] W. Veitschegger and C.-H. Wu, "Robot accuracy analysis based on kinematics," *IEEE Trans. Robot. Autom.*, vol. RA-2, no. 3, pp. 171–179, Sep. 1986.

[7] H. Zhuang, Z. S. Roth, and F. Hamano, "A complete and parametrically continuous kinematic model for robot manipulators," *IEEE Trans. Robot. Autom.*, vol. 8, no. 4, pp. 451–463, Aug. 1992.
[8] R. M. Murray, Z. Li, and S. S. Sastry, *A Mathematical Introduction to Robotic Manipulation*. Boca Raton, FL, USA: CRC Press, 1994.
[9] K. Okamura and F. C. Park, "Kinematic calibration using the product of exponentials formula," *Robotica*, vol. 14, pp. 415–422, 1996.
[10] Y. Wu, C. Li, J. Li, and Z. Li, "Comparative study of robot kinematic calibration algorithms using a unified geometric framework," in *Proc. IEEE Conf. Robot. Autom.*, 2014, pp. 1393–1398.
[11] Y. Lou, T. Chen, Y. Wu, Z. Li, and S. Jiang, "Improved and modified geometric formulation of POE based kinematic calibration of serial robots," in *Proc. IEEE/RSJ Intell. Robot. System.*, 2009, pp. 5261–5266.
[12] C. Li, Y. Wu, and Z. Li, "Identifiability and improvement of adjoint error approach for serial robot calibration," in *Proc. IEEE Conf. Robot. Autom.*, 2014, pp. 1361–1366.
[13] X. Yang, L. Wu, J. Li, and K. Chen, "A minimal kinematic model for serial robot calibration using POE formula," *Robot. Comput. Integr. Manuf.*, vol. 30, no. 3, pp. 326–334, 2014.
[14] I. Chen, G. Yang, C. Tan, and S. Yeo, "Local POE model for robot kinematic calibration," *Mechanism Mach. Theory*, vol. 36, nos. 11/12, pp. 1215–1239, 2001.
[15] K. Schröer, S. L. Albright, and M. Grethlein, "Complete, minimal and model-continuous kinematic models for robot calibration," *Robot. Comput. Integr. Manuf.*, vol. 13, no. 1, pp. 73–85, 1997.
[16] L. Everett and A. Suryohadiprojo, "A study of kinematic models for forward calibration of manipulators," in *Proc. IEEE Robot. Autom.*, 1988, vol. 2, pp. 798–800.
[17] L. J. Everett and T. W. Hsu, "The theory of kinematic parameter identification for industrial robots," *J. Dyn. Syst. Meas. Control*, vol. 110, no. 1, pp. 96–100, 1988.
[18] W. Khalil, M. Gautier, and C. Enguehard, "Identifiable parameters and optimum configurations for robots calibration," *Robotica*, vol. 9, no. 01, pp. 63–70, 1991.
[19] R. He, Y. Zhao, S. Yang, and S. Yang, "Kinematic-parameter identification for serial-robot calibration based on POE formula," *IEEE Trans. Robot.*, vol. 26, no. 3, pp. 411–423, Jun. 2010.
[20] G. Chen, H. Wang, and Z. Lin, "Determination of the identifiable parameters in robot calibration based on the POE formula," *IEEE Trans. Robot.*, vol. 30, no. 5, pp. 1066–1077, Oct. 2014.
[21] D. Baker, "Some topological problems in robotics," *Math. Intell.*, vol. 12, no. 1, pp. 66–76, 1990.
[22] B. Hall, *Lie Groups, Lie Algebras, and Representations: An Elementary Introduction*, vol. 222. New York, NY, USA: Springer, 2003.
[23] W. M. Boothby, *An Introduction to Differentiable Manifolds and Riemannian Geometry*, 2nd ed. Amsterdam, NY, USA: Academic Press, 2003.
[24] H. Pottmann, M. Peternell, and B. Ravani, "An introduction to line geometry with applications," *Comput. Aided Design*, vol. 31, no. 1, pp. 3–16, 1999.
[25] R. Abraham, J. E. Marsden, and T. Ratiu, *Manifolds, Tensor Analysis, and Applications*, vol. 75, 2nd ed. New York, NY, USA: Springer, 1988.
[26] J. Hilgert and K.-H. Neeb, *Structure and Geometry of Lie Groups*. New York, NY, USA: Springer, 2012.
[27] J. Meng, G. Liu, and Z. Li, "A geometric theory for analysis and synthesis of sub-6 dof parallel manipulators," *IEEE Trans. Robot.*, vol. 23, no. 4, pp. 625–649, Aug. 2007.
[28] J. Hervé, "The Lie group of rigid body displacements, a fundamental tool for mechanism design," *Mechanism Mach. Theory*, vol. 34, no. 5, pp. 719–730, 1999.
[29] Z. Li, J. Gou, and Y. Chu, "Geometric algorithms for workpiece localization," *IEEE Trans. Robot. Autom.*, vol. 14, no. 6, pp. 864–878, Dec. 1998.
[30] Y. Wu, H. Wang, and Z. Li, "Quotient kinematics machines: Concept, analysis, and synthesis," *J. Mechanisms Robot.*, vol. 3, no. 4, 2011, Art. no. 041004.
[31] J.-H. Borm and C.-H. Meng, "Determination of optimal measurement configurations for robot calibration based on observability measure," *Int. J. Robot. Res.*, vol. 10, no. 1, pp. 51–63, 1991.
[32] A. Nahvi and J. M. Hollerbach, "The noise amplification index for optimal pose selection in robot calibration," in *Proc. IEEE Conf. Robot. Autom.*, 1996, pp. 647–654.
[33] M. A. Meggiolaro and S. Dubowsky, "An analytical method to eliminate the redundant parameters in robot calibration," in *Proc. IEEE Robot. Autom.*, 2000, vol. 4, pp. 3609–3615.
[34] H. Zhuang and Z. S. Roth, *Camera-Aided Robot Calibration*. Boca Raton, FL, USA: CRC Press, 1996.

Cheng Li received the B.S. degree in control science and engineering from Zhejiang University, Hangzhou, China, in 2011 and the Ph.D. degree in electronic and computer engineering from Hong Kong University of Science and Technology, Hong Kong, China, in 2015.

He is a Scientist with ABB Corporation Research Center, Shanghai, China. His research interests include robot calibration, motion control, parallel robots, and robot applications.

Yuanqing Wu received the B.Sc. degree in mechanical engineering and the Ph.D. degree in mechatronics engineering, both from Shanghai Jiaotong University, Shanghai, China, in 2001 and 2009, respectively.

He was first a Research Assistant and later a Research Associate with the Electronic and Computer Engineering Department, Hong Kong University of Science and Technology, Hong Kong. He is currently a Contract Researcher with the Department of Industrial Engineering, University of Bologna, Bologna, Italy. His research interests include kinematic geometry, mechanism theory, parallel robots, geometric control, and geometric algebra computing.

Harald Löwe received the Diploma (Hons.) degree in mathematics in 1990 and the Dr. rer. nat. degree (*summa cum laude*) in 1994, both from Technical University of Braunschweig, Braunschweig, Germany, and the Habilitation degree in 2001.

He is a Professor with the Department of Mathematics, Technical University of Braunschweig. He was a Visiting Professor with University of La Laguna, Santa Cruz de Tenerife, Spain, and University Henri Poincaré, Nancy, France. He recently joined Beijing Union University, Beijing, China, as a Guest Professor. He is concerned with high school projects in mathematics. His research interests include geometry, geometric methods in robotics, and the design of spiral bevel gears.

Dr. Löwe is the Chief Editor of *Mathematikinformation*. He received the Heinrich-Büssing Prize for outstanding research in 2002.

Zexiang Li (M'83–F'08) received the B.S. degree (Hons.) in electrical engineering and economics from Carnegie Mellon University (CMU), Pittsburgh, PA, USA, in 1983, and the M.A. degree in mathematics and the Ph.D. degree in electrical engineering and computer science from University of California (UC), Berkeley, CA, USA, in 1985 and 1989, respectively.

From 1989 to 1990 he was with ALCOA, the Robotics Institute of CMU, and with the AI Laboratory, Massachusetts Institute of Technology, Cambridge, MA, USA. From 1990 to 1992 he was an Assistant Professor with the Courant Institute, New York University, New York, NY, USA. In 1992, he joined the Department of Electronic and Computer Engineering, Hong Kong University of Science and Technology (HKUST), Hong Kong, where he is currently a Professor. He founded the Automation Technology Center and co-founded the Robotics Institute, HKUST. He is a Co-Founder of Googol Technology and DJI. His research interests include multifingered robotic hand, parallel manipulators, workpiece localization and inspection, motion control, precision assembly, and unmanned aerial vehicles.

Dr. Li received the ALCOA Foundation Fellowship in 1979 and the E. Anthony Fellowship in 1983. He received the University Scholar Award from CMU in 1983, the E.I. Jury Award from UC Berkeley in 1989, the Research Initiation Award from National Science Foundation (USA) in 1990, the Outstanding Young Researcher Award (Class B) from National Natural Science Foundation of China in 2000, the LEAD Award from AMI, USA in 2001, and the Natural Science Award (third class) from China in 1997.